



Published in final edited form as:

*J Am Chem Soc.* 2017 September 13; 139(36): 12758–12772. doi:10.1021/jacs.7b07124.

## Mechanistic Studies of Copper-Catalyzed Asymmetric Hydroboration of Alkenes

Yumeng Xi, John F. Hartwig\*

Division of Chemical Sciences, Lawrence Berkeley National Laboratory, and Department of Chemistry, University of California, Berkeley, California 94720, United States

### Abstract

Mechanistic studies of the copper-catalyzed asymmetric hydroboration of vinylarenes and internal alkenes are reported. Catalytic systems with both DTBM-SEGPHOS and SEGPHOS as the ligands have been investigated. With DTBM-SEGPHOS as the ligand, the resting state of the catalyst, which is also a catalytic intermediate, for hydroboration of 4-fluorostyrene is a phenethylcopper(I) complex ligated by the bisphosphine. This complex was fully characterized by NMR spectroscopy and X-ray crystallography. The turnover-limiting step in the catalytic cycle for the reaction of vinylarenes is the borylation of this phenethylcopper complex with pinacolborane (HBpin) to form the boronate ester product and a copper hydride. Experiments showed that the borylation occurs with retention of configuration at the benzylic position.  $\beta$ -Hydrogen elimination and insertion of the alkene to reform this phenethylcopper complex is reversible in the absence of HBpin but is irreversible during the catalytic process because reaction with HBpin is faster than  $\beta$ -hydrogen elimination of the phenethylcopper complex. Studies on the hydroboration of a representative internal alkene, *trans*-3-hexenyl 2,4,6-trichlorobenzoate, which undergoes enantio- and regioselective addition of HBpin catalyzed by DTBM-SEGPHOS, KO<sup>t</sup>Bu, and CuCl, also was conducted, and these studies revealed that a DTBM-SEGPHOS-ligated copper(I) dihydridoborate complex is the resting state of the catalyst in this case. The turnover-limiting step in the catalytic cycle for hydroboration of the internal alkene is insertion of the alkene into a copper(I) hydride formed by reversible dissociation of HBpin from the copper dihydridoborate species. With SEGPHOS as the ligand, a dimeric copper hydride was observed as the dominant species during the hydroboration of 4-fluorostyrene, and this complex is not catalytically competent. DFT calculations provide a view into the origins of regio- and enantioselectivity of the catalytic process and indicate that the charge on the copper-bound carbon and delocalization of charge onto the aryl ring control the rate of the alkene insertion and the regioselectivity of the catalytic reactions of vinylarenes.

\*Corresponding Author: jhartwig@berkeley.edu.

Supporting Information

The Supporting Information is available free of charge on the ACS Publications website at DOI: 10.1021/jacs.7b07124.

Experimental procedures, characterization data, Cartesian coordinates for all computed structures (PDF)

X-ray crystallographic data for **6** (CIF)

X-ray crystallographic data for **7** (CIF)

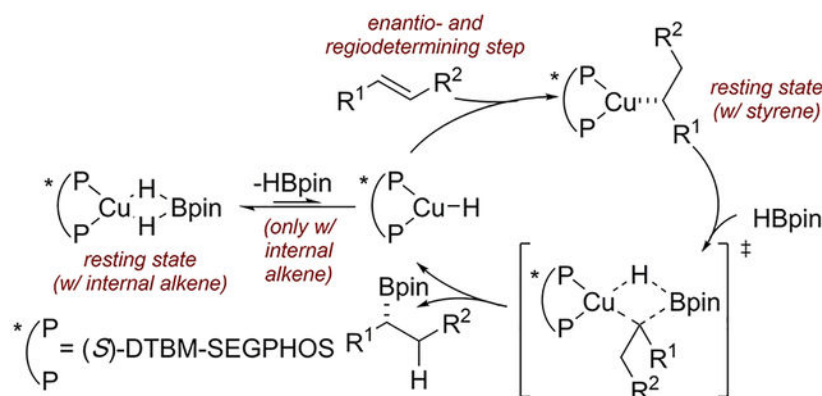
X-ray crystallographic data for **12'** (CIF)

X-ray crystallographic data for **16** (CIF)

X-ray crystallographic data for **27** (CIF)

The authors declare no competing financial interest.

## Graphical Abstract



## INTRODUCTION

The hydroboration of alkenes is a classic and synthetically valuable organic transformation that converts alkenes to organoboron compounds. Because organoboron compounds are versatile synthetic intermediates for constructing carbon–carbon and carbon–heteroatom bonds,<sup>1</sup> hydroboration has been investigated extensively since its discovery.<sup>2</sup> Many boron reagents have been designed to modulate the chemo-, regio-, and stereoselectivity of the reaction,<sup>3</sup> including those that create stereogenic centers at which the carbon–boron bond is formed.<sup>4,5</sup>

Catalytic hydroboration reactions<sup>6,7</sup> occur with selectivities<sup>8–10</sup> that often complement those of noncatalyzed reactions. For example, Evans reported examples of hydroboration reactions, catalyzed by iridium and rhodium complexes, that were directed by the coordinating functional groups within the substrate, leading to high regio- and diastereoselectivity.<sup>11,12</sup> Catalysts for enantioselective hydroboration also have been developed.<sup>13</sup> Following the initial reports by Burgess and Hayashi,<sup>9,14</sup> Takacs reported rhodium systems that catalyze directed hydroboration of disubstituted<sup>15</sup> and trisubstituted alkenes<sup>16,17</sup> with high regio- and enantioselectivity.

The first copper-catalyzed asymmetric hydroboration of alkenes was reported by Yun in 2009 (Scheme 1A).<sup>18,19</sup> A combination of a copper(I) precatalyst, base, and chiral, nonracemic bisphosphine catalyzed hydroboration of vinylarenes with high regio- and enantioselectivity. Later, the reaction was extended to the hydroboration of vinyl boronates<sup>20</sup> and norbornadienes<sup>21</sup> by the same group. In both cases, high enantioselectivity was achieved.

Last year, we reported a copper-catalyzed enantioselective hydroboration of nonconjugated internal alkenes<sup>22</sup> with high regioselectivity that complements that of Takacs' rhodium system (Scheme 1B).<sup>15–17</sup> In contrast to many olefin functionalizations catalyzed by transition metals,<sup>10,23–29</sup> functionalizations of alkenes catalyzed by copper complexes occur without competing isomerization of the alkene or migration of an alkylmetal intermediate along the alkyl chain. Experimental observations and DFT calculations implied that the

regioselectivity is controlled by the electronic effects of the polar functional groups proximal to the alkene moiety. Aliphatic secondary boronates prepared by this method were converted to a diverse set of functionalized compounds efficiently with complete or predominant conservation of the enantiomeric excess of the products from the hydroboration.<sup>30</sup>

Yun and co-workers have investigated the mechanism of copper-catalyzed hydroboration by DFT calculations.<sup>31,32</sup> A copper(I) hydride<sup>33–36</sup> was invoked as the key intermediate in these reactions. A simple mechanism is depicted in Scheme 1C. A copper(I) hydride inserts an alkene to form an alkylcopper intermediate, which undergoes stereoretentive transmetalation with HBpin to afford the product and regenerate the copper hydride. DFT calculations provided a rationalization for the greater reactivity of catalysts containing bidentate, electron-rich phosphines than of catalysts containing monodentate phosphines.<sup>31</sup>

We have conducted experiments, in addition to computations, on the catalytic cycle to determine the effects of ligands and substrates on the identity of the catalyst, the relative rates of individual steps of the cycle, and the steps that influence regio- and stereoselectivity. Our previous study<sup>22</sup> showed that the reactions occurred in high yields only with alkenes that bear inductively electron-withdrawing groups proximal to the alkene moiety. Unactivated 1,2-disubstituted alkenes underwent hydroboration in lower yields under harsher conditions (higher catalyst loading, large excess of alkene) than did nonconjugated 1,2-disubstituted alkenes that are electronically activated. Understanding the mechanism may enable the development of catalysts that are capable of engaging substrates that are less reactive than vinylarenes and polarized 1,2-disubstituted alkenes. Furthermore, understanding the origin of the absence of chain walking of the copper catalyst during the hydroboration<sup>37</sup> may help design new catalysts that possess this unusual property.

Herein, we report detailed mechanistic studies on the copper-catalyzed asymmetric hydroboration of vinylarenes and internal alkenes. A series of catalytically relevant copper(I) complexes have been synthesized and fully characterized. The reactivity and catalytic competency of these complexes have been evaluated, and kinetic studies show that the turnover-limiting and reversible steps of the reaction depend on the type of alkene. Additional experiments have been conducted to probe the origin of the stereochemical outcome of the reaction, and DFT calculations provide a view into the origin of regio- and enantioselectivity.

## RESULTS AND DISCUSSION

### Effects of the Ligands on Catalyst Activity.

During our initial discovery of copper-catalyzed hydroboration of nonconjugated internal alkenes,<sup>22</sup> we found that the reactivity of the catalyst strongly depends on subtle changes to the structure of the ancillary ligand. The catalyst formed from (*S*)-DTBM-SEGPHOS was highly active for the hydroboration of vinylarenes and nonconjugated internal alkenes containing an electron-withdrawing group, such as *trans*-3-hexenyl 2,4,6-trichlorobenzoate. However, the catalyst derived from (*S*)-SEGPHOS did not catalyze the hydroboration of the internal alkene.

We hypothesized that the difference in reactivity between the catalysts derived from these two ligands resulted,<sup>38,39</sup> at least in part, from the difference of the form of the corresponding copper hydride complexes. Almost all copper hydride complexes that are relevant to homogeneous catalysis and that have been characterized previously are oligomers, with nuclearities ranging from dimers to hexamers.<sup>34</sup> Complexes in higher-order forms were also reported.<sup>33</sup> Copper hydride complexes ligated by biaryl bisphosphines have not been isolated,<sup>40–46</sup> and full characterization of a monomeric copper hydride ligated by an extremely bulky N-heterocyclic carbene ligand was only recently reported by Bertrand.<sup>47,48</sup> To understand how the ligand structure influences the reactivity of the active catalyst, we investigated complexes in hydroboration reactions containing copper complexes of DTBM-SEGPHOS and of SEGPHOS.

### Mechanistic Studies on Hydroboration Catalyzed by DTBM-SEGPHOS-Ligated Copper(I).

Our mechanistic studies encompass reactions of two model substrates shown in Scheme 2: 4-fluorostyrene (**1**),<sup>49</sup> and the internal alkene *trans*-3-hexenyl 2,4,6-trichlorobenzoate (**2**). These reactions are discussed below; the kinetic behavior and resting states of the catalysts are much different for the two catalytic reactions. The following sections describe the identity of the complexes in the reactions, the kinetic behavior of the systems, the stoichiometric reactions of the complexes, the stereochemical outcome of the reactions, and a full energy profile assessed by DFT calculations.

### Synthesis and Characterization of Complexes That Are Competent Intermediates in the Hydroboration of Vinylarene **1** with HBpin.

Monitoring the hydroboration reaction of vinylarene **1** with 1.05 equiv of HBpin at room temperature by <sup>31</sup>P NMR spectroscopy revealed two major species. The reaction was conducted in a 1:1 mixture of cyclohexane and benzene as solvent; the reaction in cyclohexane alone was too fast to monitor at room temperature.

Two species were observed throughout the reaction. The major species, which was determined to account for about 70% of the phosphorus content, is free (*S*)-DTBM-SEGPHOS. This result shows that, during the catalytic reaction, most of the ligand remains unbound, a result which is consistent with Buchwald's observation in a related hydroamination system.<sup>50</sup> A minor species was observed as a singlet at –7.2 ppm in the <sup>31</sup>P NMR spectra; this chemical shift is consistent with a complex containing the ligand bound to copper. <sup>19</sup>F NMR spectra of the reactions contained a small but distinct peak at –129.9 ppm, in addition to peaks corresponding to reagent **1** and product **3**. Because the complex corresponding to this resonance contains a fluorine atom, we hypothesized that the species corresponding to the small resonance at –129.9 ppm could be the phenethylcopper(I) complex (DTBM-SEGPHOS)Cu[1-(4-fluoro)phenethyl] (**5**). Although most of the phosphine ligand remains unbound during the hydroboration of **1**, our mechanistic study focused on the structure and reactions of the ligated copper species, rather than identifying the NMR-silent unligated copper species. The unligated species, such as CuH aggregates, are unlikely to lie on the catalytic cycle because the enantioselectivity of the catalytic process is high.

To gain further information on the identity of phenethyl complex **5**, we synthesized this complex independently by insertion of vinylarene **1** into copper hydride **8**, as shown in Scheme 3. To do so, hydride **8** was prepared by borylation of methylcopper complex **7** with HBpin or addition of hydride sources to copper chloride **6**. Methylcopper complex **7** was prepared from chloride **6**.

(*S*)-DTBM-SEGPHOSCuCl (**6**) was isolated in 94% yield from CuCl and (*S*)-DTBM-SEGPHOS. Single-crystal X-ray diffraction of **6** revealed a monomeric structure, with a trigonal planar geometry at the copper(I) center (Figure 1). Unlike the dimeric structure<sup>51,52</sup> of copper complexes ligated by biaryl bisphosphines that are smaller than DTBM-SEGPHOS, complex **6** is monomeric, presumably due to the severe steric congestion imposed by the bulky DTBM-SEGPHOS ligand.

Methyl copper<sup>53–58</sup> complex **7** was isolated in 86% yield from the reaction of **6** with methyllithium at  $-35$  °C. Although complex **7** is stable as a solid at room temperature for at least 24 h, it decomposed in benzene under argon in ambient light overnight, and a solution of **7** reacted with air instantaneously. The solid-state structure of **7** contained a slightly unsymmetrical Y-shaped copper(I) center like that in chloride **6** (Figure 2).

The reaction of equimolar amounts of methyl complex **7** and HBpin did not yield a ligated copper hydride **8**. Instead, only free ligand was observed, suggesting that the hydride complex ligated by DTBM-SEGPHOS is not stable in solution. This instability we observed contrasts Lipshutz's proposal that the copper hydride ligated by DTBM-SEGPHOS is a stable monomer.<sup>44</sup> The reaction of chloride **6** with potassium triethylborohydride<sup>41</sup> formed a copper triethylborohydride complex,<sup>59</sup> rather than terminal hydride **8**. Attempts to sequester the BEt<sub>3</sub> moiety of the copper triethylborohydride by adding various bases led to decomposition.

Thus, phenethylcopper complex **5** was prepared by generating a DTBM-SEGPHOS-ligated copper hydride formed in the presence of the vinylarene (Scheme 4). The reaction of **6**, NaHBET<sub>3</sub>, and vinylarene **1** in cyclohexane afforded **5** in 66% yield. A higher yield (78% by <sup>19</sup>F NMR spectroscopy) was obtained by treating a mixture of methylcopper complex **7** with vinylarene **1** and HBpin in cyclohexane.

Phenethyl complex **5** was stable in the solution for several hours before decomposition to generate free ligand began to be observed by NMR spectroscopy. A quartet at 2.85 ppm and a doublet at 1.73 ppm in the <sup>1</sup>H NMR spectrum of **5** with a mutual coupling constant of 7.2 Hz clearly indicated the presence of a phenethyl moiety. A correlation between the quartet and the doublet was confirmed by 1H COSY experiments. By analogous methods, a series of phenethylcopper complexes (**9–12**) were synthesized from **7**, HBpin, and the corresponding vinylarenes (Scheme 4). Like complex **5**, complexes **9–12** were fully characterized in solution by multinuclear NMR spectroscopy.

We found that a minor product (**5'**, **9'–12'**) formed along with the major phenethylcopper complex in all the cases. Moreover, solutions containing an approximately 19:1 ratio of **5** to **5'** converted slowly over time to a lower ratio of the two complexes. After 1 h, a 13:1 ratio

of isomers was observed, and after 13 h a 4:1 ratio was observed (vide infra). The minor species consistently exhibited a  $^{31}\text{P}$  NMR signal just 1 ppm downfield of that corresponding to the major species and a  $^{19}\text{F}$  NMR signal just 0.3 ppm upfield of that corresponding to the major species.

We proposed that the minor species ( $5'$ ,  $9'-12'$ ) are the diastereomers of **5** and **9-12**, with the configuration at the benzylic carbon opposite to those in complexes **5** and **9-12**. Concomitant decomposition of the complexes prevented full equilibration and determination of the equilibrium ratio of diastereomers.

The connectivity of the phenethylcopper(I) complex was unambiguously established by X-ray diffraction analysis (Figure 3) of a DTBM-SEGPHOS-ligated 1-(2-fluoro)phenethylcopper complex. This complex is a trigonal planar  $d^{10}$ -Cu(I) complex, with a structure similar to that of methyl complex **7**, but with a slightly longer metal-carbon bond. The phenethyl group in this complex is bound in an  $\eta^1$ -coordination mode, like that of the NHC-ligated benzylcopper complexes reported by Sadighi<sup>60</sup> and Schomaker.<sup>61</sup> The fluorine atom on the aromatic ring is 3.47 Å from the copper center, indicating the absence of a potential interaction between these two atoms.

Although the bulk sample of the crystals formed by recrystallization consisted of a mixture of the two diastereomers **12** and **12'**, the crystal solved by X-ray diffraction contained a single diastereomer with an (*S*) configuration at the benzylic carbon. Because the epimerization of the phenethylcopper complexes occurred during the workup and recrystallization process, even at  $-40$  °C, we were unable to obtain a sufficient quantity of diastereomerically pure crystals to characterize a bulk sample of a single diastereomer of the phenethylcopper complex in solution.

However, information on the configuration of the benzylic carbon in the kinetic and thermodynamic isomers of the phenethylcopper complexes was gained by DFT. We calculated the relative energies of the two diastereomeric phenethylcopper complexes and the transition states leading to them (Scheme 5). The results show that the activation barrier leading to the parent phenethylcopper complex **14** is 3.4 kcal/mol lower than that leading to its diastereomer **14'**. However, **14** is higher in energy than **14'** by 2.1 kcal/mol. These DFT calculations are consistent with formation of one diastereomer that isomerizes to another over time and imply that the benzylic center in **5** and **9-12** has an (*R*) configuration and that in the more stable diastereomers  $5'$  and  $9'-12'$  has the same (*S*) configuration that was observed by X-ray diffraction. Further evidence for these assignments is given later in this paper.

## Synthesis and Characterization of Complexes That Are Catalytically Relevant to the Hydroboration of Internal Alkene **2**.

Monitoring a hydroboration reaction of internal alkene **2** with 1.2 equiv of HBpin catalyzed by a combination of CuCl, KO<sup>t</sup>Bu, and (*S*)-DTBM-SEGPHOS at room temperature revealed the presence of two phosphorus-containing species. As observed for the reaction of vinylarene **1**, the major phosphorus-containing species, which corresponded to 90% of the total phosphine content, is free (*S*)-DTBM-SEGPHOS. A broad  $^{31}\text{P}$  NMR resonance

corresponding to a minor species, dihydridoborate complex **15**, was observed at 8.0 ppm in cyclohexane.

Dihydridoborate complex **15** was generated independently by treating methylcopper complex **7** with 2 equiv of HBpin in toluene-*d*<sub>8</sub> at -78 °C. Complex **15** formed in 79% yield, as determined by <sup>1</sup>H NMR spectroscopy. The solution of **15** is stable at or below 0 °C. Above 0 °C, the clear pale-yellow solution turned bright orange-red, and the <sup>31</sup>P NMR spectrum contained resonances indicating decomposition, most likely forming a dimeric copper hydride complex, as evidenced by a pentet signal in the <sup>1</sup>H NMR spectrum (see the Supporting Information (SI)). Because this thermal instability of **15** prevented isolation in pure form, complex **15** was characterized by a series of solution NMR spectroscopic methods.

<sup>11</sup>B NMR experiments provided strong evidence that complex **15** is a dihydridoborate complex. The proton decoupled <sup>11</sup>B{<sup>1</sup>H} NMR spectrum of **15** at -60 °C contained a sharp singlet at 8.8 ppm (Figure 4a), whereas the proton coupled <sup>11</sup>B NMR spectrum at -60 °C consisted of a triplet with <sup>1</sup>J<sub>H-B</sub> = 72 Hz, implying that the boron atom is bound to two hydrides. The substantially upfield<sup>62-66</sup> <sup>11</sup>B chemical shift of **15** (8.8 ppm), relative to that of the free HBpin (28.0 ppm), is indicative of a four-coordinate boron center, like that in a dihydridoborate complex. Chemical shifts downfield of the corresponding free borane have been observed for  $\sigma$ -borane<sup>67-69</sup> and boryl complexes.

At room temperature, dihydridoborate complex **15** and HBpin exchange rapidly on the NMR time scale, resulting in a very broad signal (25.5 ppm,  $\omega_{1/2}$  = 620 Hz). At temperatures below 0 °C, the broad signal was resolved into two peaks, one corresponding to **15** and the other to HBpin. 2D-<sup>11</sup>B EXSY NMR spectra acquired at -10 °C showed a correlation between **15** and HBpin, confirming that the borane units that are free and contained within the dihydroborate complex are exchanging and that this exchange is rapid (Figure 4b). Rate constants for the exchange measured by 2D-<sup>11</sup>B EXSY spectroscopy with concentrations of HBpin varying over a factor of 20 were indistinguishable, showing that the exchange process is zero order in HBpin. These data imply that complex **15** fragments to form HBpin and (*S*)-DTBM-SEGP<sub>2</sub>HOSCuH (**8**) with a half-life of approximately 8 ms.

To gain more detailed information on the coordination of a borohydride to the (DTBM-SEGP<sub>2</sub>HOS)Cu fragment, copper-(I) tetrahydridoborate complex **16** was prepared. Complex **16** was synthesized from **6** and excess sodium borohydride in 80% yield. The <sup>11</sup>B{<sup>1</sup>H} NMR chemical shift for **16** is -28 ppm, which is indicative of a four-coordinate boron atom. Indeed, the solid-state structure of **16** revealed a tetrahedral copper(I) center with the borohydride bound in a  $\kappa^2$  fashion (Figure 5). Complex **16** is thermally stable in solution and in the solid state; heating **16** in THF for 2 h at 65 °C did not lead to any decomposition. Consistent with this stability, complex **16** does not catalyze the hydroboration of vinylarene **1** or internal alkene **2** with HBpin.

To compare the structures of dihydroborate **15** and tetrahydridoborate **16**, we calculated the structure of **15** by DFT with the B3LYP functional and 6-31g(d)/SDD basis sets. Consistent with our NMR studies, the most stable structure of **15** contains a tetrahedral coordination

of the copper and the boron (Scheme 6; see Supporting Information for details). DFT calculations also suggest that coordination of HBpin to (*S*)-DTBM-SEGPHOSCuH (**8**) is exothermic in both gas phase and solution. However, the coordination of HBpin to (*S*)-DTBM-SEGPHOSCuH to form **15** is calculated to be exergonic by only 0.8 kcal/mol in solution. This small energy for formation of the complex between **8** and HBpin is consistent with the rapid exchange of the HBpin in dihydridoborate **15** with free HBpin by dissociation of HBpin from **15** to form hydride **8**.

### Evaluation of the Kinetic Competency of Observed Copper Complexes.

The kinetic relevance of phenethylcopper **5** and copper dihydridoborate **15** was investigated by monitoring the catalytic hydroboration of vinylarene **1** and internal alkene **2**, respectively. Complexes **5** and **15** were generated in situ from methyl complex **7** for these studies. As shown in Figures S8 and S9, the reactions catalyzed by **5** and **15** generated from **7** are much faster than those catalyzed by the combination of CuCl, KO<sup>t</sup>Bu, and (*S*)-DTBM-SEGPHOS. These data show that **5** and **15** are kinetically competent to be intermediates in the catalytic reactions of the two alkenes.

### Determination of Empirical Rate Law.

The empirical rate laws of the hydroboration of vinylarene **1** and internal alkene **2** with HBpin were determined by the method of initial rates with methylcopper **7** as the catalyst<sup>70</sup> (see Supporting Information). Kinetic experiments on the reaction of **1** with HBpin indicate that the hydroboration of **1** is first-order in [HBpin] and [Cu], but zero-order in vinylarene [**1**] (Figure S6, eq 1). These data, like our data on the resting state of the catalyst, are consistent with turnover-limiting borylation of a phenethylcopper intermediate, rather than insertion of the vinylarene into a copper hydride.

$$\begin{aligned} &\text{rate law for hydroboration of } \mathbf{1} \\ &\text{rate} = k_1[\text{Cu}][\text{HBpin}] \end{aligned} \tag{1}$$

$$\begin{aligned} &\text{rate law for hydroboration of } \mathbf{2} \\ &\text{rate} = \frac{k_1 k_2 [\text{Cu}][\text{alkene}]}{k_{-1}[\text{HBpin}] + k_2[\text{alkene}]} \end{aligned} \tag{2}$$

$$\begin{aligned} &\frac{1}{k_{\text{obs}}} = \frac{1}{k_1} + \frac{k_{-1} [\text{HBpin}]}{k_1 k_2 [\text{alkene}]} \\ &\text{(double reciprocal form)} \end{aligned} \tag{3}$$

Kinetic experiments on the reaction of internal alkene **2** with HBpin showed that the orders in the reagents for this reaction are different from those for the reaction of vinylarene **1** with HBpin. The reaction of **2** is inverse order in [HBpin], positive order in [**2**], and first-order

in [Cu], as revealed by linear graphs of  $1/\text{rate}$  vs [HBpin] and  $1/\text{rate}$  vs  $1/[2]$  (Figure S7). Equation 2 shows the rate law derived from the kinetic study, and eq 3 shows the double reciprocal form of the rate equation. These data, in combination with the observation of an adduct of a copper hydride and HBpin as the resting state, indicate that one molecule of HBpin dissociates from the resting state prior to the turnover-limiting step and that the turnover-limiting step is insertion of the alkene into a copper hydride.

### Insertion of Alkenes into Hydride **8** Generated from Methyl Complex **7** and HBpin.

To investigate the elementary steps in the proposed catalytic cycle (Scheme 1C) and to determine how these steps control the overall catalysis, we studied each step individually. As shown in Scheme 4, the reaction of vinylarene **1** with methyl complex **7** and HBpin forms phenethylcopper complex **5**. This reaction occurs within 1 min at room temperature. In contrast, no alkylcopper product was detected from the reaction of internal alkene **2** with **7** and HBpin. Our data on the exchange of the borane in complex **15** with free HBpin imply that the reaction of **7** with HBpin generates hydride **8**, which rapidly reacts with the vinylarene to form the final product phenethylcopper **5**. The lack of reaction of **2** with a 1:1 mixture of **7** and HBpin leads to decomposition of the copper hydride generated from methylcopper complex **7** and HBpin (vide supra).

The potential reversibility of the insertion of alkenes into copper hydrides could affect the origin of enantioselectivity of the hydroboration process. To probe the reversibility of alkene insertion during the catalytic reactions, we performed an isotope-labeling experiment (Scheme 7). The reaction of styrene- $d_8$  with HBpin catalyzed by methylcopper **7** was monitored by both  $^1\text{H}$  and  $^2\text{H}$  NMR spectroscopy. If the alkene insertion were reversible and fast, incorporation of hydrogen atoms into styrene- $d_8$  would be detected.<sup>50</sup> However, such incorporation of hydrogen was not observed; **17** was the only product of the reaction, implying that insertion of the alkene is irreversible in the catalytic hydroboration of vinylarenes.

This irreversibility contrasts the observed epimerization<sup>71</sup> of phenethylcopper compounds from the kinetic to thermodynamic diastereomers (vide supra). Thus, we compared the time scale of the epimerization to that of the borylation of an alkylcopper complex. The epimerization of phenethylcopper **5** to **5'**, as determined by  $^{19}\text{F}$  NMR spectroscopy in cyclohexane (Scheme 8), occurred over the time scale of hours, whereas the stoichiometric reaction between 4-fluorostyrene and an equimolar amount of **5** and HBpin occurred to completion within 10 min (vide infra). Therefore, the epimerization by reversible deinsertion and reinsertion of the alkene occurs in the absence of HBpin, but deinsertion is slower than reaction of the phenethylcopper complex with HBpin. These relative rates prevent epimerization of the phenethyl intermediate during these hydroborations of vinylarenes catalyzed by copper complexes of DTBM-SEPHOS.

Finally, to assess how the electronic properties of the alkene influence the rate of insertion, we performed a competition experiment between 4-trifluoromethylstyrene and 4-methoxystyrene (Scheme 9). Quantitative formation of  $\text{CF}_3$ -substituted phenethylcopper **9** was observed from reaction of in situ generated copper hydride **8** with the two alkenes.

Because the reaction of the alkene with a DTBM-SEGPHOS-ligated copper hydride is much faster than deinsertion, the observation of trifluoromethyl-substituted **9** implies that the ratio of products from this experiment is a kinetic selectivity and that insertion of an electron-poor alkene is much faster than insertion of an electron-rich alkene (Scheme 9).

### Reaction of Alkylcopper Complexes with HBpin.

Because the reaction of the alkylcopper complex with borane is proposed to be the product-forming step of the catalytic cycle, we investigated stoichiometric reactions of isolated alkylcopper(I) complexes with HBpin.

The reaction of methylcopper complex **7** was conducted as a benchmark of the reaction of alkylcopper complexes with boranes. Complex **7** reacted with HBpin at room temperature to afford MeBpin in 87% yield, as determined by  $^1\text{H}$  NMR spectroscopy. Both phenethylcopper complexes **5** and **9** reacted with HBpin at room temperature to afford the corresponding secondary boronates, indicating that phenethylcopper complexes are competent to be intermediates in the catalytic cycle (Scheme 10).

The relative rate of the reaction of alkylcopper complexes with HBpin was evaluated. The reaction of methylcopper **7** with HBpin occurred within seconds, even at  $-78\text{ }^\circ\text{C}$ . At room temperature, the reaction of 4-fluoro phenethylcopper complex **5** with HBpin occurred to over 95% conversion after 10 min, whereas the reaction of 4-trifluoromethyl phenethyl complex **9** with HBpin occurred to about 50% conversion after 10 min. Therefore, the relative rates of the borylation are  $\mathbf{7} \gg \mathbf{5} > \mathbf{9}$ .

Although we cannot conduct the reaction of HBpin with the putative secondary alkyl complex generated from insertion of the internal alkene into a copper hydride (*vide supra*), we presume that the rate of reaction of this secondary alkyl complex lies between that of the methylcopper complex and that of the less electron-rich secondary phenethylcopper complexes.

### Stereochemistry of the Individual Steps of the Mechanism for Hydroboration.

High enantioselectivity is obtained from the catalytic hydroboration with a wide range of alkenes. To understand the origins of this high enantioselectivity, we investigated the stereochemical outcome of each step in the proposed catalytic cycle.

The alkene insertion is turnover limiting during the reaction of internal alkene **2** and, therefore, determines the enantioselectivity and regioselectivity of the catalytic hydroboration. However, the insertion of vinylarene **1** occurs before the turnover-limiting reaction of HBpin with the phenethylcopper complex.

Several mechanistic scenarios could account for the observed enantioselectivity and the absolute configuration of the products (Scheme 11). The enantioselectivity could be controlled by an irreversible alkene insertion step or the relative energies of transition states for the borylation of the copper alkyl complex. In the latter case, the enantioselectivity would result from Curtin–Hammett control, and the alkene insertion must be reversible. Because our studies on the alkene insertion demonstrated that this step is irreversible during

the catalytic process, the absolute configuration of the product of the catalytic process results from the stereoselectivity of the insertion step and the degree of retention or inversion of configuration during the borylation of the resulting alkylcopper complex.

The catalytic reaction could occur by stereoretentive borylation of phenethylcopper **5** or by stereoinvertive borylation of **5'**. Our data on reactions of vinylarenes are consistent with reaction of the kinetically formed diastereomer **5** with HBpin to form the (*R*) enantiomer of the product. Because our DFT calculation predicted that the thermodynamically more stable diastereomer has the (*S*) configuration and the kinetically formed diastereomer has the (*R*) configuration, the reaction of HBpin with the phenethylcopper complex and, by analogy, with the alkylcopper complex would occur with retention of configuration.

To avoid uncertainties in this argument, due to its basis on our DFT calculations, we distinguished more directly between reactions of HBpin with inversion or retention of configuration by determining the relative configuration of the product from the hydroboration of a trisubstituted alkene, such as **19**. Hydroboration of trisubstituted alkene **19**, followed by oxidative workup and TBS deprotection, afforded diol **19-OH** in 32% yield with exclusive diastereoselectivity (Scheme 12). The relative configuration of the stereogenic centers in **19-OH** was confirmed to be *anti* by comparing its <sup>1</sup>H NMR spectrum to those previously reported. Because the oxidation of an enantioenriched boronate by NaOH/H<sub>2</sub>O<sub>2</sub> has been well established to be stereoretentive, and alkene insertion into metal hydrides occurs by *syn*-addition,<sup>72</sup> the borylation of the alkylcopper intermediate must be *stereoretentive*.<sup>73</sup> This result is consistent with the result of Yun on the hydroboration of a deuterium-labeled styrene derivative,<sup>32</sup> and the stereoretentive borylation is consistent with the observation of only phenethylcopper **5**, not **5'**, throughout the hydroboration of vinylarene **1**.

Second, we determined the stereochemical outcome of the stoichiometric borylation experimentally (Scheme 13). The 19:1 mixture of diastereomers (**5/5'**) formed from methylcopper complex **7**, HBpin, and 4-fluorostyrene was allowed to react with HBpin. The ee value (90%) of the boronate product **3** was assessed by HPLC after oxidative workup. The starting 19:1 mixture of **5** and **5'** and the observed ee value for the product of the reaction of this mixture of diastereomers are consistent with a borylation reaction that is stereospecific.

The absolute configuration of the product **3** from the reaction of phenethylcopper **5** and HBpin is (*R*), as shown in Scheme 13. Because the results from the hydroboration of alkene **19** indicate that the borylation is stereoretentive, the benzylic configuration of **5** must be (*R*). This configuration determined experimentally is consistent with our predicted configuration for the kinetically formed diastereomer by DFT calculations (*vide supra*).

### DFT Computational Studies of the Full Catalytic Cycles To Form All Isomeric Products.

Earlier in this paper we presented DFT computations on the insertion of styrene into hydride **8** to gain information on the configuration of the benzylic carbon in the thermodynamic and kinetic stereoisomers of phenethylcopper complexes **14** and **14'** (Scheme 5). In this section, we provide the full free energy profiles for the hydroboration of styrene and *trans*-2-

butene.<sup>74</sup> Previously, Yun and co-workers<sup>31</sup> investigated the mechanism of the reaction and how the ligand controls the catalytic efficiency by DFT calculations.<sup>75</sup> Our computational results here demonstrate how the enantio- and regioselectivity of the reactions are controlled and how the identity of the alkene influences each elementary step in the catalytic cycle.

Scheme 14 illustrates the calculated reaction pathway for hydroboration of styrene catalyzed by the DTBM-SEGPHOS-ligated copper complex, leading to all three possible isomeric products (*R*)-**21**, (*S*)-**21**, and linear **22**. The pathway labeled in red represents the reaction that leads to branched product (*R*)-**21**, the major enantiomer and constitutional isomer of the hydroboration of styrene. The path labeled in blue represents the reaction that leads to the minor enantiomer of the branched product (*S*)-**21**. The path labeled in black represents the reaction that leads to the linear product **22**.

The computed energies shown in the reaction coordinate predict that the turnover-limiting step is the borylation of the phenethylcopper species; the activation barrier for this step is higher than that for the alkene insertion step. This computational result is consistent with our kinetic studies and observation of phenethylcopper complex **5** throughout the hydroboration of vinylarene **1**. In addition, the calculations predict that the alkene insertion is irreversible because the activation barrier for the forward reaction, borylation of a phenethylcopper intermediate (20.0 kcal/mol through **13-TS**), is smaller than the barrier for the reverse reaction, alkene deinsertion (24.5 kcal/mol). These calculated energies also imply that the alkene insertion is the enantioselectivity- and regioselectivity-determining step, as determined experimentally.

Scheme 15 shows the reaction coordinates for the hydroboration of styrene (shown in red) and *trans*-2-butene (shown in blue) together. Consistent with the results from our kinetic experiments, the calculations imply that alkene insertion is the turnover-limiting step of the hydroboration of the internal alkene. This change in turnover-limiting step results from differences in the relative activation energies of the alkene insertion and the borylation of the resulting alkylcopper complex for reactions of the two types of alkenes. The activation barrier for insertion of *trans*-2-butene is higher than that for insertion of styrene, and the barrier for borylation of the copper–alkyl bond is lower than that for borylation of the copper–phenethyl bond.

To determine how electronic and steric effects control the alkene insertion, we calculated the activation barrier for insertion of propene (Scheme 16) and compared the factors controlling the barrier for this reaction to those for insertions of vinylarenes. Unlike the insertion of styrene for which 2,1-insertion is favored over 1,2-insertion, the insertion of propene favors 1,2-insertion over 2,1-insertion. The 1,2-insertion of propene is favored by 4.0 kcal/mol. The barrier to both 1,2- and 2,1-insertion of propene was computed to be significantly higher than that for 2,1-insertion of styrene, indicating that the electron-withdrawing phenyl group of the styrene causes the barrier for the insertion to be substantially lower than the barrier for insertion of propene. The barrier for 2,1-insertion of propene is close to that for insertion of *trans*-2-butene, indicating that the additional methyl group on the alkene does not significantly affect the barrier to insertion into the copper hydride.

Natural bond orbital (NBO) analysis provides a rationalization for why 2,1-insertion of styrene is favored over 1,2-insertion (Scheme 17). The preference for 2,1-insertion of styrene is not a result of potential  $\pi$ - $\pi$  interaction between the ligand and the styrene or potential formation of an  $\eta^3$ -phenethylcopper species. The transition states and products for the insertion lack interactions between the aryl groups of the ligand and styrene, and both structures contain  $\eta^1$ -phenethyl ligands without copper-arene interactions.

Instead, the results summarized in Scheme 17 show that the charges of the C-H and CH<sub>2</sub> units, as determined by NBO analysis, account for the relative stabilities of the transition states and products. The computed charge on the methine and methylene units of the transition states at which the Cu-C bond is forming (C(2)H for **13-TS**; C(1)H<sub>2</sub> for **13-I-TS**) is lower in **13-TS** leading to the branched phenethylcopper **14** than it is in **13-I-TS** leading to the linear phenethylcopper **14-I**. The NBO analysis shows that the phenyl ring of the styrene in **13-TS** shares the negative charge to a greater extent than it does in **13-I-TS**. The computed charges on the *ortho* (C(4)H, C(8)H) and *para* (C(6)H) C-H units in **13-TS** were substantial, whereas those on the *meta* (C(5)H and C(7)H) C-H units were nearly zero. A similar distribution of charges was found by computation at these positions in the insertion products **14** and **14-I**, although the charges on the copper-bound carbon and the *ortho* and *para* carbons on the aryl ring are larger than those in the transition state. These results suggest that delocalization of the negative charge from the benzylic carbon atom of **13-TS** to the adjacent phenyl ring<sup>76</sup> leads to the lower barrier for 2,1-insertion of the styrene and greater stability of the product of 2,1-insertion of the vinylarene.

This conclusion is consistent with the experimental observation that insertion of an electron-poor styrene is faster than the insertion of an electron-rich one. The transition state for the insertion should be stabilized more by an aryl ring containing an electron-withdrawing group in the former case than by an aryl ring containing an electron-donating group. Because the barrier for 1,2-insertion of styrene (18.8 kcal/mol) is computed to be very close to that for 1,2-insertion of propene (18.7 kcal/mol), our calculation provides a clear view of how electronic effects control the regioselectivity of the hydroboration of vinylarenes in the absence of metal-arene interactions.

The enantioselectivity<sup>77</sup> of the hydroboration is controlled by the relative energy (3.4 kcal/mol) of the two diastereomeric transition states **13-TS** and **13'-TS** for the insertion of styrene. The structures of **13-TS** and **13'-TS** can be visualized by quadrant diagrams (Scheme 18). For **13-TS**, the phenyl group of the styrene is located in the light gray regions, where axial aryl groups of the ligand are positioned. In contrast, for **13'-TS**, the phenyl group of the styrene is located in the dark gray regions, where equatorial aryl groups of the ligand are positioned. Because the equatorial aryl groups of the ligand are proximal to the coordinated styrene, a severe steric interaction between the equatorial aryl group and the phenyl group of the styrene was observed in **13'-TS**. This large difference in steric interactions within **13-TS** and **13'-TS** clearly leads to the observed enantioselectivity.

The activation energies for the borylation<sup>78</sup> of a series of alkylcopper species were assessed by DFT calculations (Scheme 19).<sup>79</sup> Consistent with our experimental results, the barrier computed for reaction of HBpin with electron-rich, less bulky alkylcopper complexes is

lower than that with electron-deficient, bulkier alkylcopper complexes. The rate for reaction of the methyl complex **7** with HBpin was too fast to measure, and the activation energy computed for the borylation of the primary phenethylcopper complex **14-I** is less than 10 kcal/mol. The computed barrier for borylation of the secondary alkylcopper species, *sec*-butyl complex **24**, is about 3 kcal/mol higher than that for borylation of the primary phenethylcopper species **14-I**. This borylation process is computed to have a higher barrier because the steric interactions between the alkyl group of **24** and HBpin in the transition state are more severe than those between HBpin and the linear phenethyl group of **14-I**. The free energy of activation for borylation of the secondary phenethylcopper complex **14** is computed to be much higher than that for borylation of the primary phenethylcopper complex **14-I** and for borylation of the *sec*-butyl complex **24**. In addition to steric effects, the lower charge on the copper-bound carbon atom of the phenethyl moiety than on the copper-bound carbon of the linear phenethylcopper complex is likely to be the origin of this large difference in activation energies.

### Mechanistic Studies on Hydroboration Catalyzed by SEGPHOS-Ligated Copper(I).

The copper catalyst ligated by (*S*)-SEGPHOS was significantly less active than that ligated by (*S*)-DTBM-SEGPHOS. To understand this difference in reactivity and, thereby, reveal features of the catalyst that lead to high activity, we investigated the hydroboration of vinylarene **1** with the catalyst formed from (*S*)-SEGPHOS.

### Synthesis and Characterization of Catalytically Relevant Complexes.

Monitoring a hydroboration reaction of **1** with HBpin catalyzed by CuCl, KO<sup>t</sup>Bu, and (*S*)-SEGPHOS in toluene at room temperature by <sup>31</sup>P NMR spectroscopy revealed multiple species at the early stage of the reaction (see Supporting Information for details). However, a broad signal at 1.9 ppm in the <sup>31</sup>P NMR spectra became dominant as the reaction progressed to around 40% conversion.

The dimeric copper hydride complex, [(*S*)-SEGPHOSCuH]<sub>2</sub> (**27**), which corresponds to the <sup>31</sup>P NMR chemical shift of 1.9 ppm, was independently synthesized by treating [(*S*)-SEGPHOSCuCl]<sub>2</sub><sup>51</sup> with sodium triethylborohydride. The <sup>1</sup>H NMR spectrum of **27** in benzene-*d*<sub>6</sub> contained a characteristic broad singlet at 2.60 ppm, which was assigned to the hydride resonance. This chemical shift is similar to that of other phosphine-ligated copper hydride complexes reported previously.<sup>44–46</sup> The corresponding copper deuteride analog was prepared, and its <sup>2</sup>H NMR spectrum contained a broad singlet at 2.60 ppm. Complex **27** is stable in solid form at room temperature for at least 6 h, but is unstable in solution. A concentrated THF or toluene solution of **27** at –40 °C decomposed overnight, and this decomposition prevented purification to afford a microanalytically pure sample.

Despite its low stability, we obtained single crystals of complex **27** suitable for X-ray diffraction. The dimeric structure of [(*S*)-SEGPHOSCuH]<sub>2</sub> in the solid state was unambiguously confirmed (Figure 6, left). In the solid state, the two copper atoms and the four phosphorus atoms are almost in one plane (the dihedral angles of P1–Cu1–Cu2–P3 and P2–Cu1–Cu2–P4 are 0.57° and 6.13°, respectively). The hydrides in the solid-state structure could not be located accurately.

Thus, the location of the hydrides was investigated by DFT calculations on the most stable structure of **27**. Calculations with a series of different functionals showed that the copper center adopts a tetrahedral geometry with a Cu–H bond length of 1.73 Å (Figure 6, right; see Supporting Information for details). This result is consistent with geometries observed for other phosphine-ligated copper hydride complexes reported previously.

### Assessment of the Catalytic Relevance of Dimeric Copper Hydride **27** to the Hydroboration of Vinylarene **1**.

To assess whether dimeric hydride complex **27** is kinetically competent to be an intermediate in the hydroboration of vinylarene **1**, we monitored the reaction by GC. The profile for the reaction catalyzed by complex **27** clearly showed that it occurs with an induction period of approximately 3 h (Scheme 20).

The hydroboration of vinylarene **1** catalyzed by complex **27** is significantly slower than that catalyzed by a combination of CuCl, KO<sup>t</sup>Bu, and (*S*)-SEGPHOS. Although the ee of the products formed by the two catalytic systems were indistinguishable, the rate and the yield of the reaction catalyzed by the complex generated in situ are higher than those of the reaction initiated with complex **27** (Scheme 20). These results suggest that complex **27** is not catalytically competent to be an intermediate and, therefore, lies off the catalytic cycle. However, the similarity of the ee values obtained for the hydroboration catalyzed by complex **27** and by the system generated in situ suggests that the dimeric copper hydride **27** generates the active catalyst, which is presumably the monomeric complex (*S*)-SEGPHOSCuH (**28**).<sup>80,81</sup> The conversion of the mixture of copper complexes observed at early stages of the reaction to complex **27** likely results from a reduction in the rate of insertion of vinylarene **1** into hydride **28** because the vinylarene is consumed by the reaction.

## SUMMARY AND DISCUSSIONS OF MECHANISTIC STUDIES

### Proposed Mechanism for Hydroboration.

Our experimental and computational studies provide unusually detailed information on the mechanism of an enantioselective, catalytic hydrofunctionalization of alkenes. The mechanism of the hydroboration of terminal vinylarenes and of the hydroboration of internal alkenes catalyzed by DTBM-SEGPHOS-ligated copper complexes that is consistent with all of our data is shown in Scheme 21. The catalytic cycle consists of two steps. The first step involves insertion of an alkene by a monomeric copper hydride to form an alkylcopper intermediate. The second step involves reaction of the alkylcopper with HBpin by a  $\sigma$ -bond metathesis mechanism to release the product and regenerate the copper hydride. This general mechanism occurs for all classes of alkenes, but the turnover-limiting step and catalyst resting state depend on the identity of the alkene.

Kinetic experiments revealed the turnover-limiting step in each proposed catalytic cycle. Phenethylcopper complex **5** was the only phosphine-ligated copper species observed during the hydroboration of vinylarene **1** with DTBM-SEGPHOS as the ligand, and the reaction of this complex with HBpin is the turnover-limiting step. In contrast, copper dihydridoborate **15** was the only phosphine-ligated copper species observed during the catalytic reaction of

the internal alkene **2**, and the turnover-limiting step is the insertion of **2** into copper hydride **8**, which is formed by reversible dissociation of HBpin from **15**.

Experiments provided information about the origins of the configurations of the copper intermediates. For the hydroboration of vinylarene **1**, our experimental data showed that the alkene insertion is reversible in the absence of HBpin but is irreversible throughout the catalytic process because reaction of the phenethylcopper complex with HBpin is faster than epimerization of the phenethylcopper complex. Thus, the migratory insertion of the alkene sets the configuration of the product. For the hydroboration of internal alkene **2**, this step is also irreversible, and the configuration of the  $\alpha$ -carbon of the alkylcopper intermediate is, again, set by the insertion.

The irreversible insertion of internal alkene **2** explains the absence of isomerization of alkylcopper intermediates through a chain-walking process in the hydroboration of **2**. The rapid conversion of the secondary alkylcopper complex to product prohibits migration of the copper along the alkyl chain by a series of deinsertion and insertion steps, even though deinsertion can occur. The computed barriers for reaction of the alkyl complexes with borane are 5–10 kcal/mol lower than the barrier for deinsertion of the alkyl complex to generate a copper hydride and the alkene.

As noted in the beginning of this paper, a portion of the copper in the system is ligated by DTBM-SEGPHOS and a portion lacks the phosphine ligand, as determined by the observation of between 3:1 and 9:1 ratios of free DTBM-SEGPHOS to ligated DTBM-SEGPHOS in systems containing a 1.1:1 ratio of ligand to copper. However, the enantioselectivity of the catalytic process is high (>95%). For this reason, reactions through the unligated copper cannot account for a significant fraction of the product, and we have shown that the intermediates we observe are kinetically and chemically competent to lie on the catalytic cycle.

### Effect of Ligand Steric Properties on the Catalytic Activity.

The size of substituents on the aryl rings in the ligand has a dramatic effect on the reactivity of the catalyst. Ligands containing bulky groups, such as *tert*-butyl groups, at the 3,5-position of the aryl rings generate more active catalysts than those containing smaller groups at these positions. For example, DTBM-SEGPHOS formed a highly active catalyst, whereas DMM-SEGPHOS, with methyl groups at the 3- and 5-position of the aryl rings in place of *tert*-butyl groups, did not form an active catalyst (Scheme 22), although the electronic properties of DTBM-SEGPHOS are similar to those of DMM-SEGPHOS. Likewise, DM-SEGPHOS shown in Scheme 22 did not form an active catalyst for hydroboration of **2**. Our mechanistic studies on reactions catalyzed by complexes of DTBM-SEGPHOS and of SEGPHOS imply that this difference in catalyst activity results from the formation of catalytically incompetent, dimeric copper hydride complexes when the ligand is smaller than DTBM-SEGPHOS. Bulky ligands, such as DTBM-SEGPHOS, cause the copper complexes to remain mononuclear.

## CONCLUSION

In summary, we report a detailed mechanistic study of the copper-catalyzed asymmetric hydroboration of alkenes. We studied the hydroboration of vinylarene **1** with both SEGPHOS and DTBM-SEGPHOS as the ligand and the hydroboration of internal alkene **2** with DTBM-SEGPHOS as the ligand. Several copper complexes have been isolated and fully characterized by X-ray diffraction and multinuclear NMR spectroscopy, and these complexes have been shown to be chemically and catalytically competent. Stoichiometric reactions provided insight into each elementary step in the catalytic cycle, and kinetic studies, along with the observation of catalytic intermediates, revealed the turnover-limiting step in the catalytic cycle. Through these experiments, we have gained insight into the origin of the enantio- and regioselectivity. DFT calculations provided additional support and explanation for the experimental data. The following specific conclusions can be drawn from these data.

1. The catalyst speciation depended on the ligand and the alkene. With SEGPHOS as ligand, dinuclear copper species are dominant, but with the bulky ligand DTBM-SEGPHOS, all of the observed copper species were monomeric. For reactions of vinylarenes, the ligated catalyst resting state is a phenethylcopper(I) species, but for reactions of internal, unconjugated alkenes, the ligated catalyst resting state is a copper dihydridoborate complex.
2. Dimeric copper hydride complexes ligated by bidentate phosphines are not kinetically competent to be part of the catalytic system. Such complexes are formed by dimerization of the active monomeric copper hydride, and this process reduces the rate of the catalysis. Catalysts in this system ligated by the bulky DTBM-SEGPHOS are highly active because they are mononuclear.
3. The hydroboration of vinylarene **1** is first-order in [Cu] and [HBpin], and zero-order in [**1**]; the hydroboration of internal alkene **2** is first-order in [Cu], inverse order in [HBpin], and positive order in [**2**]. Thus, the turnover-limiting step of the reactions of vinylarenes is the reaction of a phenethylcopper complex with HBpin, and the turnover-limiting step of the reactions of internal, unconjugated alkene is insertion of the alkene into a copper hydride generated by reversible dissociation of HBpin from DTBM-SEGPHOS-ligated dihydroborate complex **15**.
4. Stoichiometric reactions of the copper hydride and alkenes showed that an electron-poor vinylarene undergoes insertion much faster than an electron-rich vinylarene, which undergoes insertion faster than an unconjugated alkene, and these relative rates were explained by DFT calculations. NBO analysis provided a clear view of how the charge on the copper-bound carbon and delocalization of charge onto the aryl ring control the rate of the alkene insertion, the regioselectivity of the reaction, and the rate of reaction with HBpin.
5. The alkene insertion is irreversible in the catalytic reactions. In the absence of HBpin, the epimerization of phenethylcopper intermediates to the corresponding diastereomers, by reversible deinsertion and insertion of the alkene, occurs

in solution. However, the epimerization of the phenethylcopper complex, and therefore deinsertion is slower than reaction of this complex with HBpin. For this reason, epimerization and chain walking do not occur during the catalytic hydroboration.

6. Studies on the alkene insertion suggest that the enantioselectivity- and regioselectivity-determining step in the catalytic cycle is alkene insertion, regardless of the alkene substrate and the ligand.<sup>82</sup>
7. The rates of the borylation of discrete alkylcopper complexes with HBpin followed the trend: electron-rich electron-poor copper complexes. The reaction occurs with retention of configuration to afford the corresponding boronates.
8. Evaluation of the effect of ligand properties on catalyst activity showed that the steric properties of the ligand dominate the reactivity of the copper catalyst. Sterically encumbered ligands form highly reactive catalysts. In particular, the steric bulk of the aryl rings of the ligand at the 3- and 5-positions affected the reactivity of the catalyst substantially by maintaining a monomeric form of the catalyst.

Overall, this study has revealed the fundamental principles that govern the efficiency of the copper catalysts for reactions with alkenes and selectivity of the alkene hydroboration. The interplay between the alkene insertion and borylation steps controls the overall catalyst speciation and reaction kinetics. More active catalytic systems are required for hydroboration of unactivated internal alkenes, and we hope an approach involving rational design of ligands through both experiment and theory will increase the rate of this process. Such studies will be the subject of future work in our laboratory.

## Supplementary Material

Refer to Web version on PubMed Central for supplementary material.

## ACKNOWLEDGMENTS

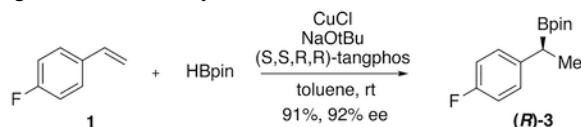
This work was supported by the Director, Office of Science, of the U.S. Department of Energy under Contract No. DE-AC02-05CH11231 and the Molecular Graphics and Computation Facility at UC Berkeley (NSF CHE-0840505) for DFT calculations. We gratefully acknowledge Dr. Hasan Celik for assistance with NMR experiments, Dr. Antonio DiPasquale for X-ray crystallography (NIH S10-RR027172), Dr. Miao Zhang in the LBL Catalysis Facility for assistance with IR experiments, and Takasago for gifts of (*S*)-DTBM-SEGPHOS and (*R*)-DMM-SEGPHOS. We thank Sophie Arlow for assistance with the preparation of the manuscript and Dr. Rhett Baillie for assistance with the X-ray diffraction study.

## REFERENCES

- (1). Matteson DS Stereodirected Synthesis with Organoboranes; Springer: Berlin, Heidelberg, 1995.
- (2). Brown HC; Rao BCS J. Am. Chem. Soc 1956, 78, 5694.
- (3). Zaidlewicz M Hydroboration; John Wiley & Sons, Inc.: 2000.
- (4). Brown HC; Singaram B Acc. Chem. Res 1988, 21, 287.
- (5). Thomas SP; Aggarwal VK Angew. Chem., Int. Ed 2009, 48, 1896.
- (6). Burgess K; Ohlmeyer MJ Chem. Rev 1991, 91, 1179.
- (7). Beletskaya I; Pelter A Tetrahedron 1997, 53, 4957.

- (8). Männig D; Nöth H *Angew. Chem., Int. Ed. Engl* 1985, 24, 878.
- (9). Hayashi T; Matsumoto Y; Ito YJ *Am. Chem. Soc* 1989, 111, 3426.
- (10). Obligacion JV; Chirik PJ *J. Am. Chem. Soc* 2013, 135, 19107. [PubMed: 24328236]
- (11). Evans DA; Fu GC *J. Am. Chem. Soc* 1991, 113, 4042.
- (12). Evans DA; Fu GC; Hoveyda AH *J. Am. Chem. Soc* 1992, 114, 6671.
- (13). Crudden CM; Edwards D *Eur. J. Org. Chem* 2003, 2003, 4695.
- (14). Burgess K; Ohlmeyer MJ *J. Org. Chem* 1988, 53, 5178.
- (15). Smith SM; Thacker NC; Takacs JM *J. Am. Chem. Soc* 2008, 130, 3734. [PubMed: 18311977]
- (16). Smith SM; Takacs JM *J. Am. Chem. Soc* 2010, 132, 1740. [PubMed: 20092272]
- (17). Shoba VM; Thacker NC; Bochat AJ; Takacs JM *Angew. Chem., Int. Ed* 2016, 55, 1465.
- (18). Noh D; Chea H; Ju J; Yun J *Angew. Chem., Int. Ed* 2009, 48, 6062.
- (19). Copper-catalyzed formal hydroboration using  $B_2pin_2$  and an alcohol, which operates by a mechanism that is distinct to the copper-catalyzed hydroboration with HBpin, also effectively affords enantioenriched boronates. For selected examples, see: (a) Lee Y; Hoveyda AH *J. Am. Chem. Soc* 2009, 131, 3160. [PubMed: 19256564] (b) Corberán R; Mszar NW; Hoveyda AH *Angew. Chem., Int. Ed* 2011, 50, 7079.
- (20). Feng X; Jeon H; Yun J *Angew. Chem., Int. Ed* 2013, 52, 3989.
- (21). Lee H; Lee BY; Yun J *Org. Lett* 2015, 17, 764. [PubMed: 25603172]
- (22). Xi Y; Hartwig JF *J. Am. Chem. Soc* 2016, 138, 6703. [PubMed: 27167490]
- (23). Johnson LK; Killian CM; Brookhart MJ *Am. Chem. Soc* 1995, 117, 6414.
- (24). Kochi T; Hamasaki T; Aoyama Y; Kawasaki J; Kakiuchi FJ *Am. Chem. Soc* 2012, 134, 16544.
- (25). Werner EW; Mei T-S; Burckle AJ; Sigman MS *Science* 2012, 338, 1455. [PubMed: 23239733]
- (26). Bair JS; Schramm Y; Sergeev AG; Clot E; Eisenstein O; Hartwig JF *J. Am. Chem. Soc* 2014, 136, 13098. [PubMed: 25171744]
- (27). Larionov E; Lin L; Guénee L; Mazet C *J. Am. Chem. Soc* 2014, 136, 16882. [PubMed: 25397681]
- (28). Vasseur A; Bruffaerts J; Marek I *Nat. Chem* 2016, 8, 209. [PubMed: 26892551]
- (29). Lata CJ; Crudden CM *J. Am. Chem. Soc* 2010, 132, 131. [PubMed: 19968306]
- (30). Leonori D; Aggarwal VK *Angew. Chem., Int. Ed* 2015, 54, 1082.
- (31). Won J; Noh D; Yun J; Lee JY *J. Phys. Chem. A* 2010, 114, 12112. [PubMed: 20968303]
- (32). Noh D; Yoon SK; Won J; Lee JY; Yun J *Chem. - Asian J* 2011, 6, 1967. [PubMed: 21523913]
- (33). Dhayal RS; van Zyl WE; Liu CW *Acc. Chem. Res* 2016, 49, 86. [PubMed: 26696469]
- (34). Jordan AJ; Lalic G; Sadighi JP *Chem. Rev* 2016, 116, 8318. [PubMed: 27454444]
- (35). Pirmot MT; Wang Y-M; Buchwald SL *Angew. Chem., Int. Ed* 2016, 55, 48.
- (36). Deutsch C; Krause N; Lipshutz BH *Chem. Rev* 2008, 108, 2916. [PubMed: 18616323]
- (37). In our previous study (see ref 22), we did not observe products that resulted from chain-walking of the copper catalyst.
- (38). Lipshutz BH *Synlett* 2009, 2009, 509.
- (39). Lipshutz BH; Noson K; Chrisman W; Lower AJ *Am. Chem. Soc* 2003, 125, 8779.
- (40). Bezman SA; Churchill MR; Osborn JA; Wormald JJ *Am. Chem. Soc* 1971, 93, 2063.
- (41). Goeden GV; Caulton KG *J. Am. Chem. Soc* 1981, 103, 7354.
- (42). Lemmen TH; Folting K; Huffman JC; Caulton KG *J. Am. Chem. Soc* 1985, 107, 7774.
- (43). Goeden GV; Huffman JC; Caulton KG *Inorg. Chem* 1986, 25, 2484.
- (44). Lipshutz BH; Frieman BA *Angew. Chem., Int. Ed* 2005, 44, 6345.
- (45). Eberhart MS; Norton JR; Zuzek A; Sattler W; Rucolo SJ *Am. Chem. Soc* 2013, 135, 17262.
- (46). Zall CM; Linehan JC; Appel AM *J. Am. Chem. Soc* 2016, 138, 9968. [PubMed: 27434540]
- (47). A DTBM-SEGPHOS-ligated copper hydride was characterized in situ by  $^1H$  NMR spectroscopy by Lipshutz, which was proposed to be a monomer. See ref 44.
- (48). Romero EA; Olsen PM; Jazzar R; Soleilhavoup M; Gembicky M; Bertrand G *Angew. Chem., Int. Ed* 2017, 56, 4024.

- (49). Yun reported the hydroboration of **1** catalyzed by a combination of CuCl, NaOtBu, and (*S,S,R,R*)-tangphos with high enantioselectivity. See ref 18.



- (50). Bandar JS; Pirmot MT; Buchwald SL J. Am. Chem. Soc 2015, 137, 14812. [PubMed: 26522837]
- (51). Lipshutz BH; Frieman B; Birkedal H Org. Lett 2004, 6, 2305. [PubMed: 15228265]
- (52). Hattori G; Sakata K; Matsuzawa H; Tanabe Y; Miyake Y; Nishibayashi YJ Am. Chem. Soc 2010, 132, 10592.
- (53). Yamamoto A; Miyashita A; Yamamoto T; Ikeda S Bull. Chem. Soc. Jpn 1972, 45, 1583.
- (54). Mankad NP; Gray TG; Laitar DS; Sadighi JP Organometallics 2004, 23, 1191.
- (55). Schaper F; Foley SR; Jordan RF J. Am. Chem. Soc 2004, 126, 2114. [PubMed: 14971946]
- (56). Goj LA; Blue ED; Delp SA; Gunnoe TB; Cundari TR; Pierpont AW; Petersen JL; Boyle PD Inorg. Chem 2006, 45, 9032. [PubMed: 17054364]
- (57). Pérez M; Fañanás-Mastral M; Bos PH; Rudolph A; Harutyunyan SR; Feringa BL Nat. Chem 2011, 3, 377. [PubMed: 21505496]
- (58). Coan PS; Folting K; Huffman JC; Caulton KG Organometallics 1989, 8, 2724.
- (59). Collins LR; Rajabi NA; Macgregor SA; Mahon MF; Whittlesey MK Angew. Chem., Int. Ed 2016, 55, 15539.
- (60). Laitar DS; Tsui EY; Sadighi JP Organometallics 2006, 25, 2405.
- (61). Schmid SC; Van Hoveln R; Rigoli JW; Schomaker JM Organometallics 2015, 34, 4164.
- (62). Chakraborty S; Zhang J; Patel YJ; Krause JA; Guan H Inorg. Chem 2013, 52, 37. [PubMed: 22591248]
- (63). Harder S; Spielmann JJ Organomet. Chem 2012, 698, 7.
- (64). Mukherjee D; Ellern A; Sadow AD Chem. Sci 2014, 5, 959.
- (65). Bontemps S; Vendier L; Sabo-Etienne S Angew. Chem., Int. Ed 2012, 51, 1671.
- (66). Hatanaka T; Ohki Y; Tatsumi K Chem. - Asian J 2010, 5, 1657. [PubMed: 20540071]
- (67). Hebden TJ; Denney MC; Pons V; Piccoli PMB; Koetzle TF; Schultz AJ; Kaminsky W; Goldberg KI; Heinekey DM J. Am. Chem. Soc 2008, 130, 10812. [PubMed: 18642912]
- (68). Lachaize S; Essalah K; Montiel-Palma V; Vendier L; Chaudret B; Barthelat J-C; Sabo-Etienne S Organometallics 2005, 24, 2935.
- (69). Schlecht S; Hartwig JF J. Am. Chem. Soc 2000, 122, 9435.
- (70). We selected methylcopper **7** as the catalyst for kinetic studies to avoid the induction period and lack of homogeneity of the hydroboration of internal alkene **2** catalyzed by the combination of CuCl, KOtBu, and (*S*)-DTBM-SEGPHOS.
- (71). Sadighi reported the isomerization of an NHC-ligated  $\beta$ -borylalkylcopper complex to the corresponding  $\alpha$ -borylalkylcopper complex through  $\beta$ -hydrogen elimination and reinsertion. See ref 60.
- (72). Hartwig JF In Organotransition Metal Chemistry: From Bonding to Catalysis; University Science Books: Sausalito, CA, 2010; p 349.
- (73). The benzylic configuration in **20** was determined to be R by comparing the optical rotation value to the literature value. The benzylic configuration in **20** is the same as that of (*R*)-1-(4-fluorophenyl)ethanol obtained from the hydroboration of **1** and oxidation of its product (*R*)-**3**, suggesting that the origin of asymmetric induction for reaction of the simple styrene **1** is similar to that of the trisubstituted alkene **19**.
- (74). Computations were conducted at the M06/6-311+g(d,p)/SDD//B3LYP/6-31g(d)/SDD level of theory, which has been applied to many copper hydride catalyzed hydrofunctionalization reactions.
- (75). Many of the results of our calculations that include solvation correction with the SMD continuum model are different from those reported by Yun and co-workers, who reported calculations in

the gas phase. We did not find that the lowest energy pathways involve dechelation of the DTBM-SEGPLHOS ligand for the borylation of phenethylcopper intermediates.

- (76). From the NBO analysis, the bond order (1.127) of the C2–C3 bond in transition state **13-TS** supports a partial delocalization of the negative charge from the C2 atom to the phenyl ring. We did not obtain an order (1.0357) for the C2–C3 bond that supports the presence of such delocalization in transition state **13-1-TS**.
- (77). The origin of enantioselectivity in a closely related hydroamination system has been probed by DFT calculations Yang Y; Shi S-L; Niu D; Liu P; Buchwald SL Science 2015, 349, 62. [PubMed: 26138973]
- (78). DFT computational studies on the borylation of phenethylcopper intermediates of the Cu-SEGPLHOS system showed that this reaction occurs by a  $\sigma$ -bond metathesis mechanism, not a pathway involving oxidative addition of the B-H bond of HBpin, followed by reductive elimination to form the C–B bond. See Supporting Information for details.
- (79). Our DFT calculations showed that both phosphorus atoms are bound to the copper in the transition state structure of the borylation. This result contrasts those of Yun and co-workers (see ref 32), who conclude that one of the phosphorus atoms is dissociated from the copper in the transition state structure for the borylation step.
- (80). Issenhuth J-T; Notter F-P; Dagonne S; Dedieu A; Bellemin-Laponnaz S Eur. J. Inorg. Chem 2010, 2010, 529.
- (81). Vergote T; Nahra F; Merschaert A; Riant O; Peeters D; Leyssens T Organometallics 2014, 33, 1953.
- (82). See Supporting Information for additional explanation.

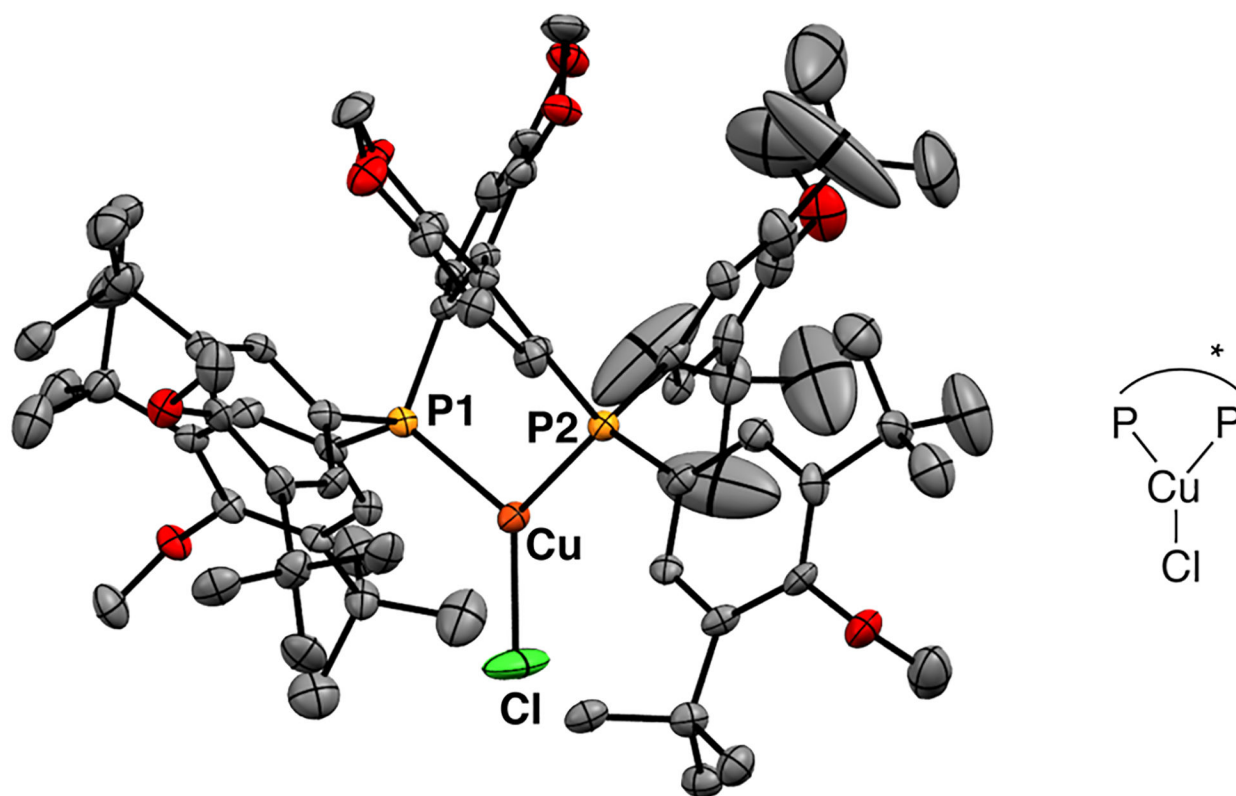


**Figure 1.** Solid-state structure of (*S*)-DTBM-SEGPHOSCuCl (**6**) determined by single crystal X-ray diffraction. The thermal ellipsoids were set to 30% probability. All hydrogen atoms were omitted for clarity. Selected bond lengths (Å): Cu–Cl = 2.178(2). Selected bond angles (deg): P1–Cu–Cl = 126.15(9), P2–Cu–Cl = 131.68(9).

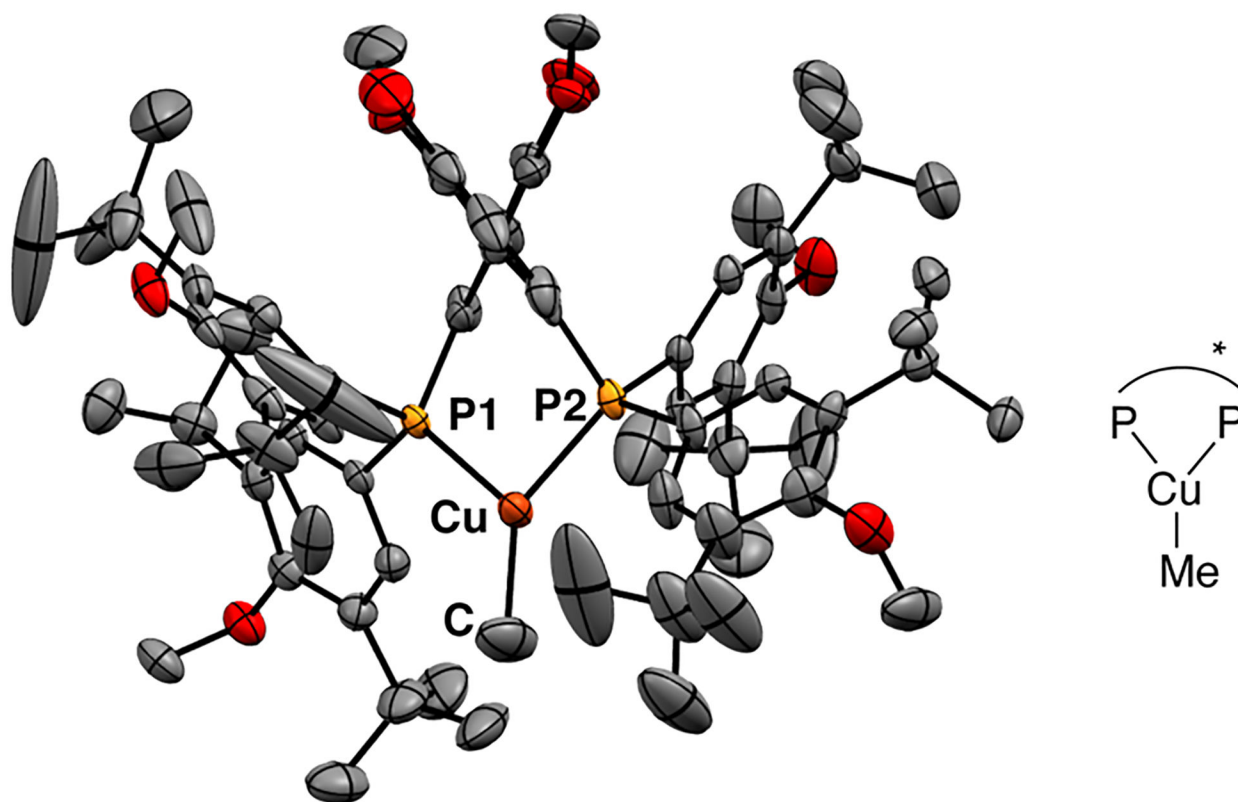


**Figure 2.** Solid-state structure of (*S*)-DTBM-SEGPHOSCuCH<sub>3</sub> (**7**) determined by single crystal X-ray diffraction. The thermal ellipsoids were set to 30% probability. All hydrogen atoms were omitted for clarity. Selected bond lengths (Å): Cu–C = 1.95(1). Selected bond angles (deg): P1–Cu–C = 128.4(3), P2–Cu–C = 133.5(3).

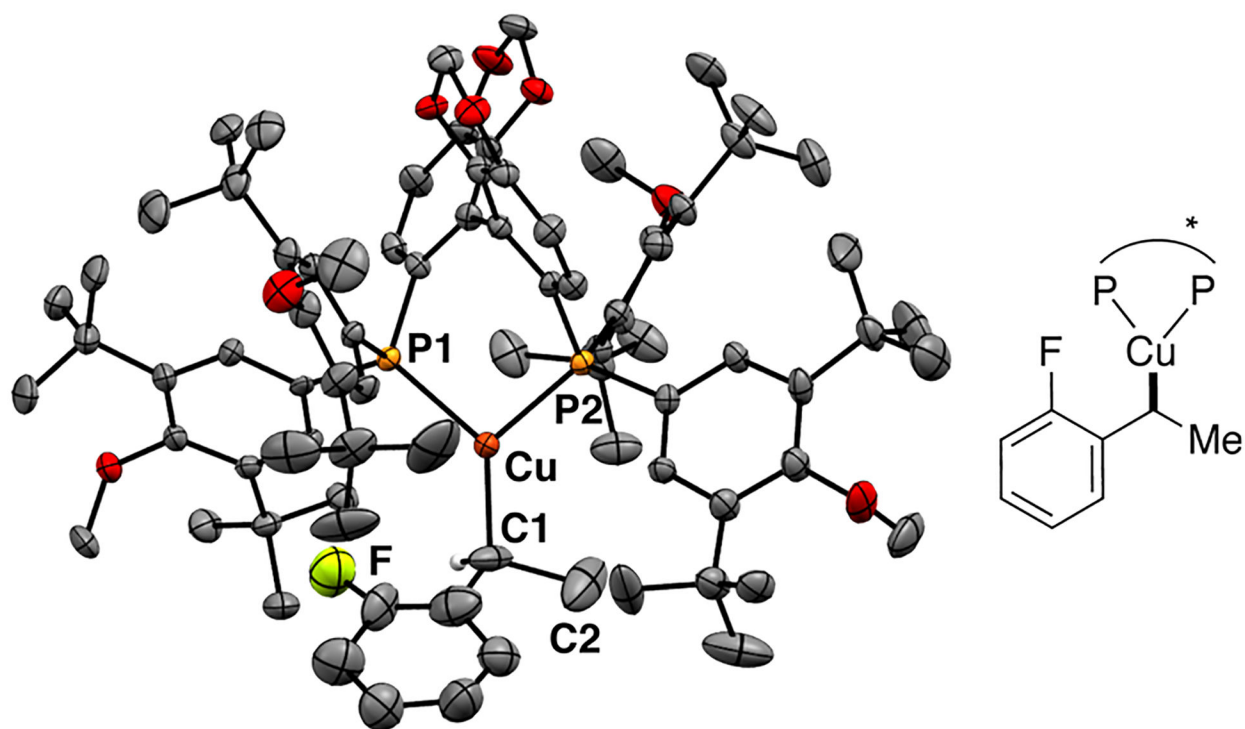


**Figure 3.**

Solid-state structure of (*S*)-DTBM-SEGPHOSCu[(*S*)-CH(2-F-C<sub>6</sub>H<sub>4</sub>)Me] determined by single crystal X-ray diffraction. The thermal ellipsoids were set to 30% probability. All hydrogen atoms except the benzylic hydrogen atom were omitted for clarity. Selected bond lengths (Å): Cu–C1 = 2.03(1). Selected bond angles (deg): P1–Cu–C1 = 130.0(4), P2–Cu–C1 = 130.8(4).

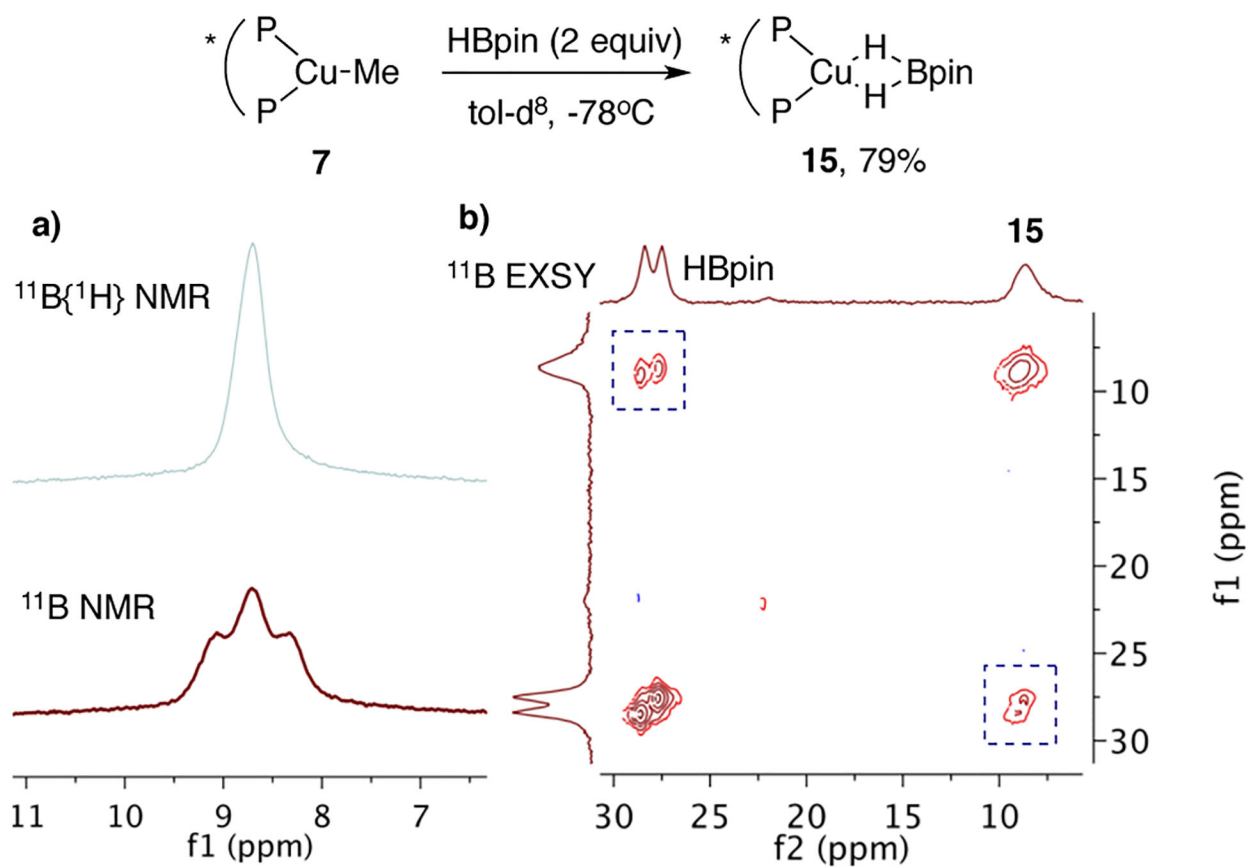


**Figure 4.**  $^{11}\text{B}$  NMR spectra of **15** (A) and 2D- $^{11}\text{B}$  EXSY NMR spectrum (B) of **15** and HBpin at  $-10^\circ\text{C}$ . The ancillary ligand on **7** and **15** is (*S*)-DTBM-SEGPHOS.

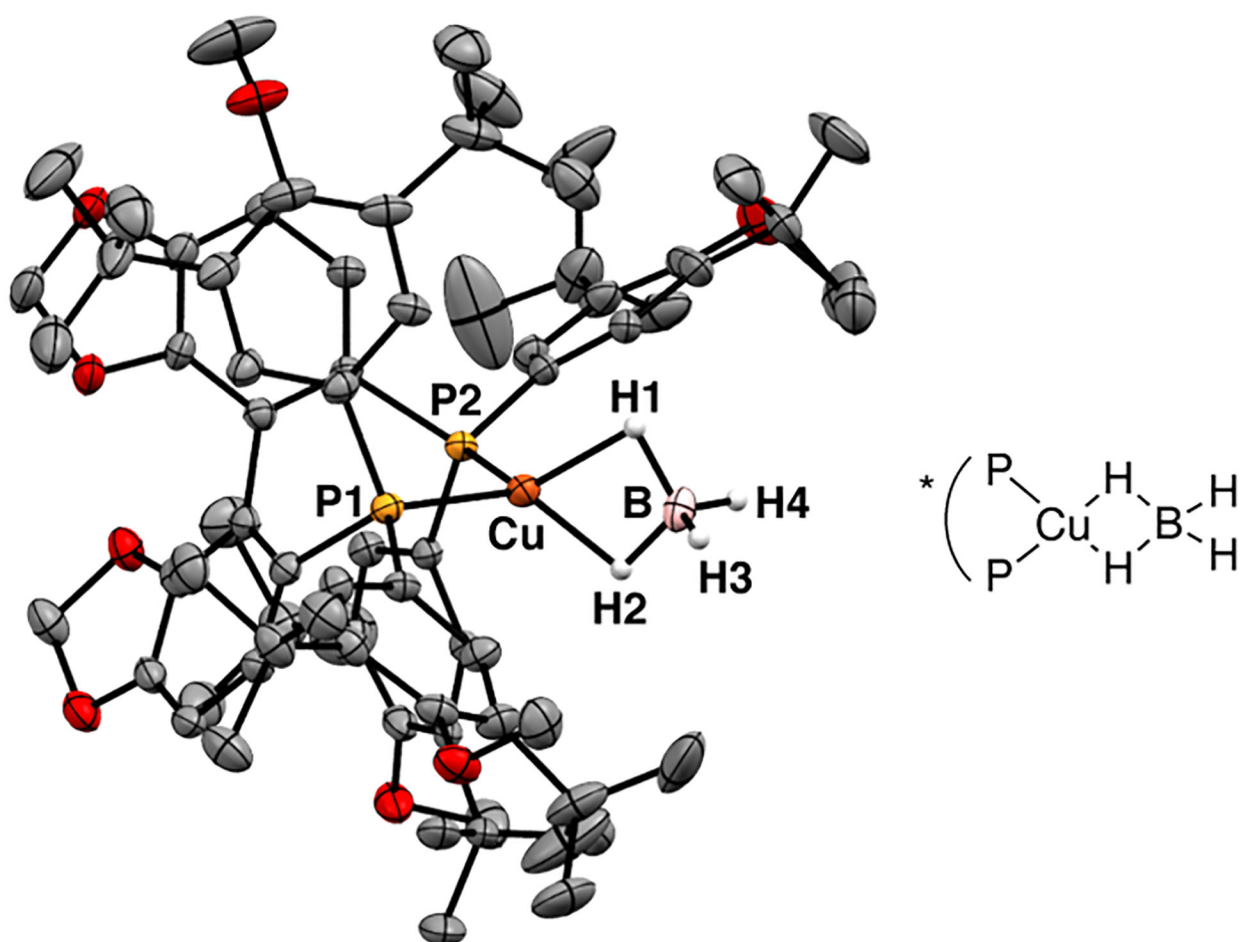


**Figure 5.** Solid-state structure of (*S*)-DTBM-SEGPBOSCuBH<sub>4</sub> (**16**) determined by single crystal X-ray diffraction. The thermal ellipsoids were set to 30% probability. All hydrogen atoms that are bound to carbon atoms were omitted for clarity.

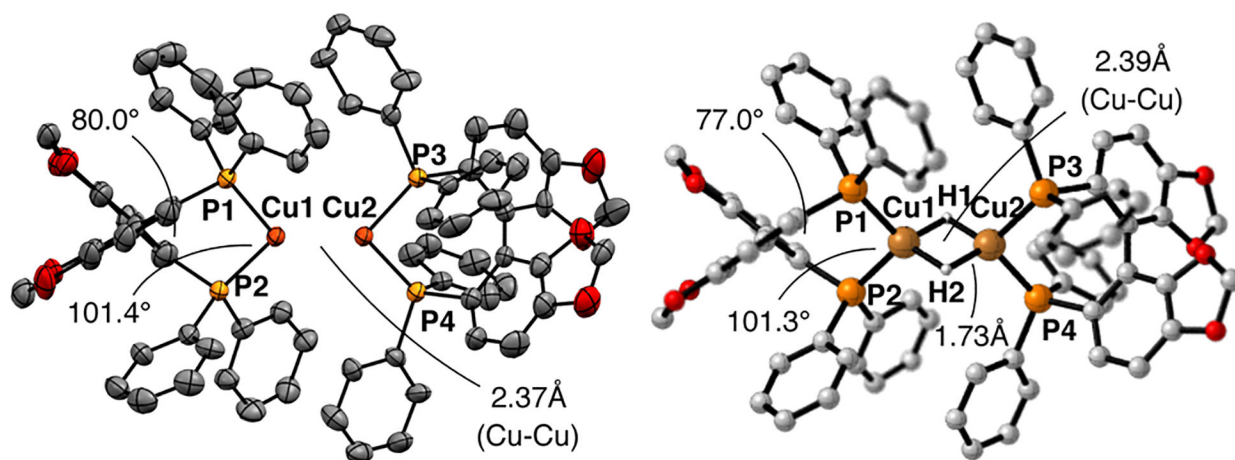
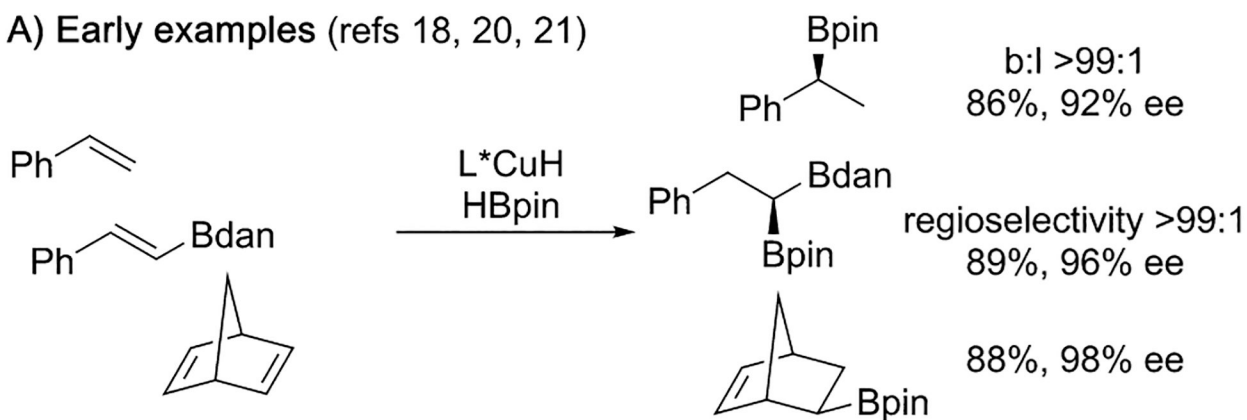
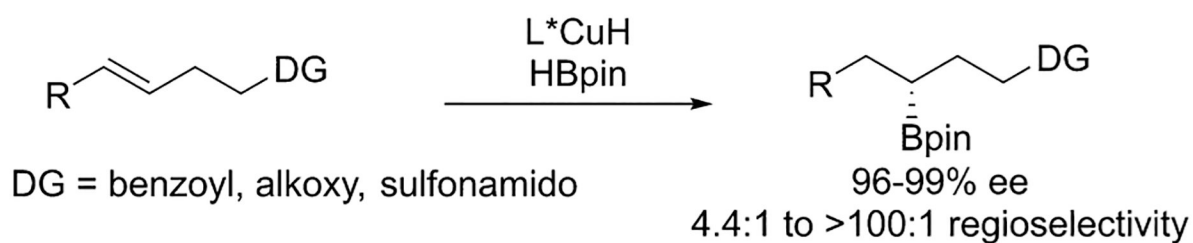


**Figure 6.** Solid-state structure determined by X-ray diffraction and DFT-computed structure of [(*S*)-SEGPHOSCuH]<sub>2</sub> (**27**). The thermal ellipsoids were set to 30% probability. All hydrogen atoms were omitted for clarity. Electron density marking the positions of the hydrides was not clearly defined. Geometry optimizations were performed at the PBE/SDD/6–31G(d) level of theory. All hydrogen atoms that are bound to carbon atoms were omitted for clarity.

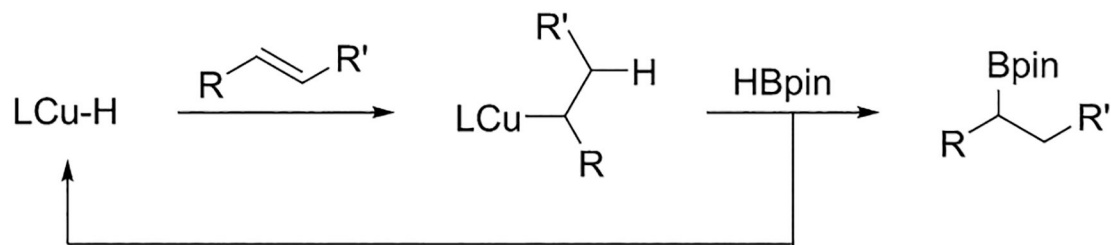
## A) Early examples (refs 18, 20, 21)



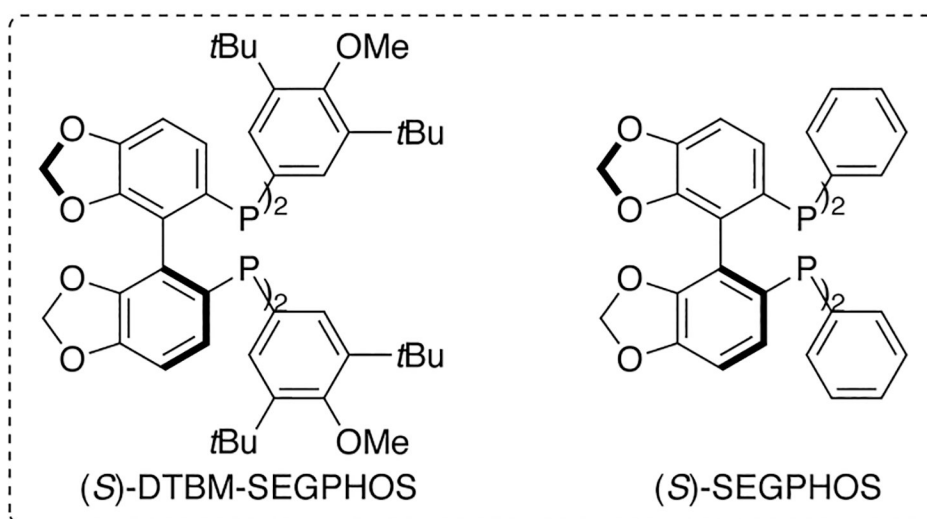
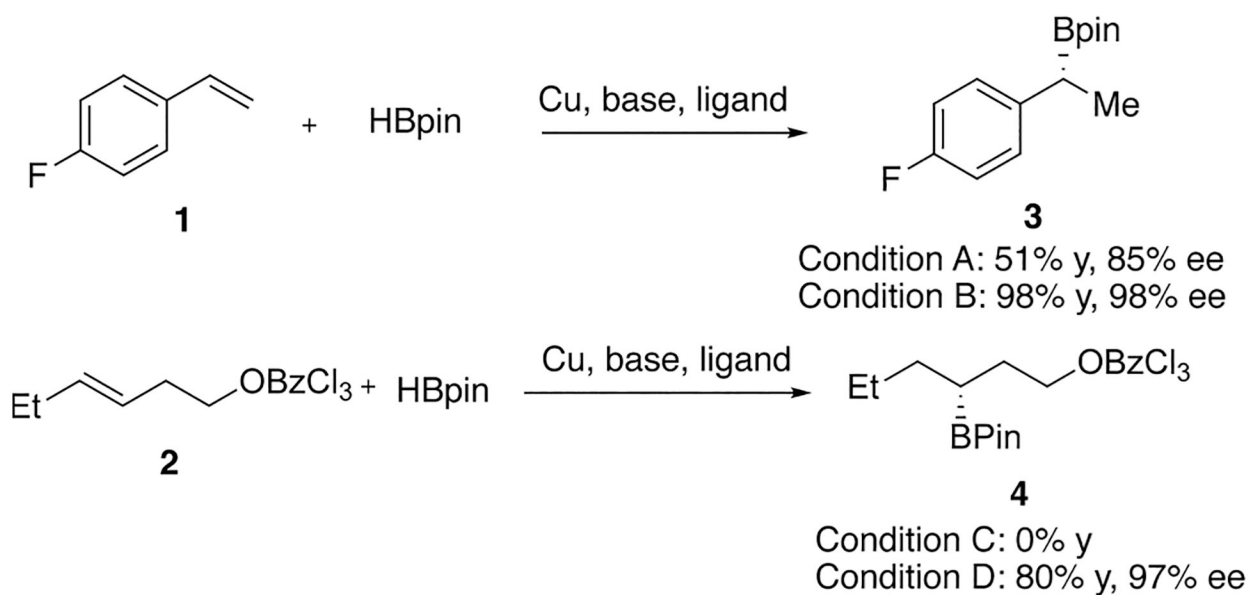
## B) Our previous work (ref 22)



## C) Proposed mechanism

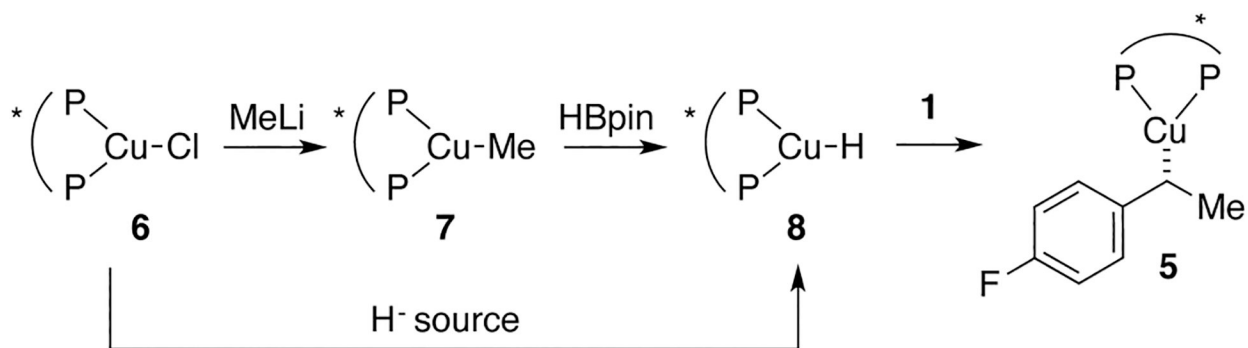


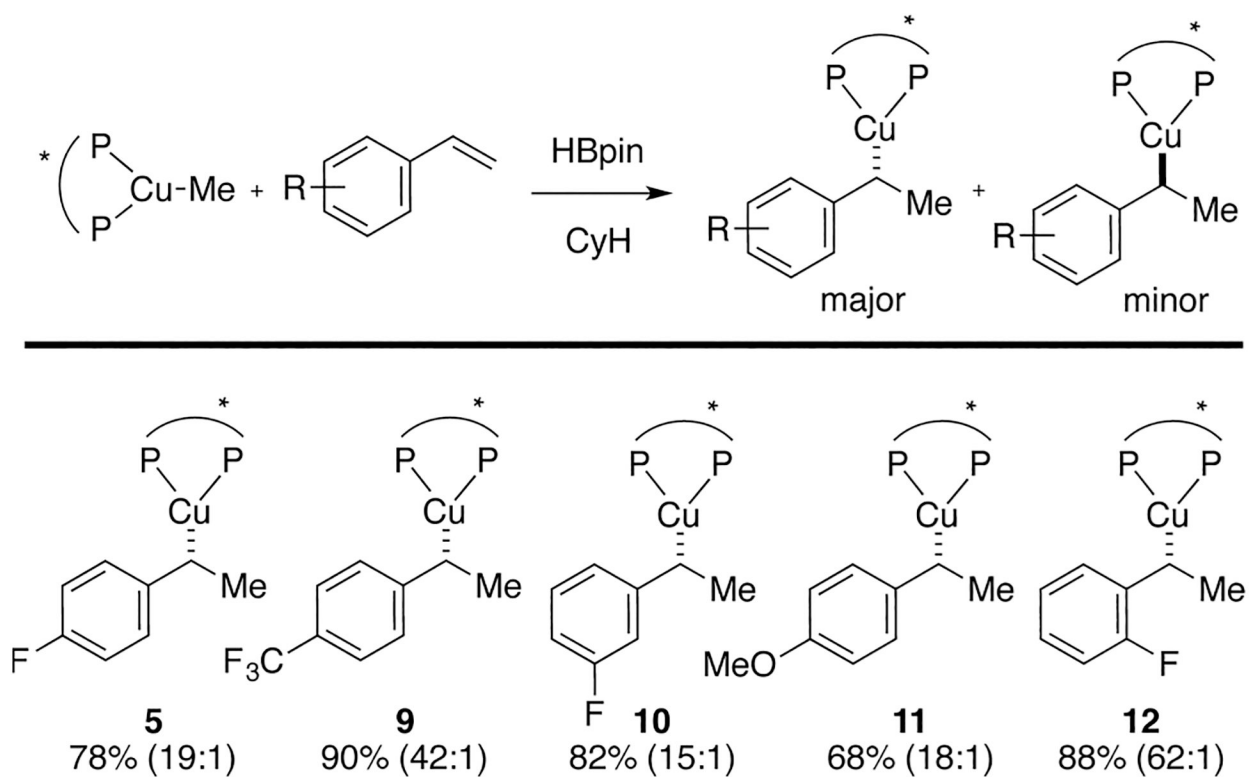
**Scheme 1.**  
Copper-Catalyzed Asymmetric Hydroboration

**Scheme 2.**

Hydroboration of 1 and 2 Catalyzed by Copper Catalysts Ligated by (*S*)-SEGPHOS and (*S*)-DTBM-SEGPHOS<sup>a</sup>

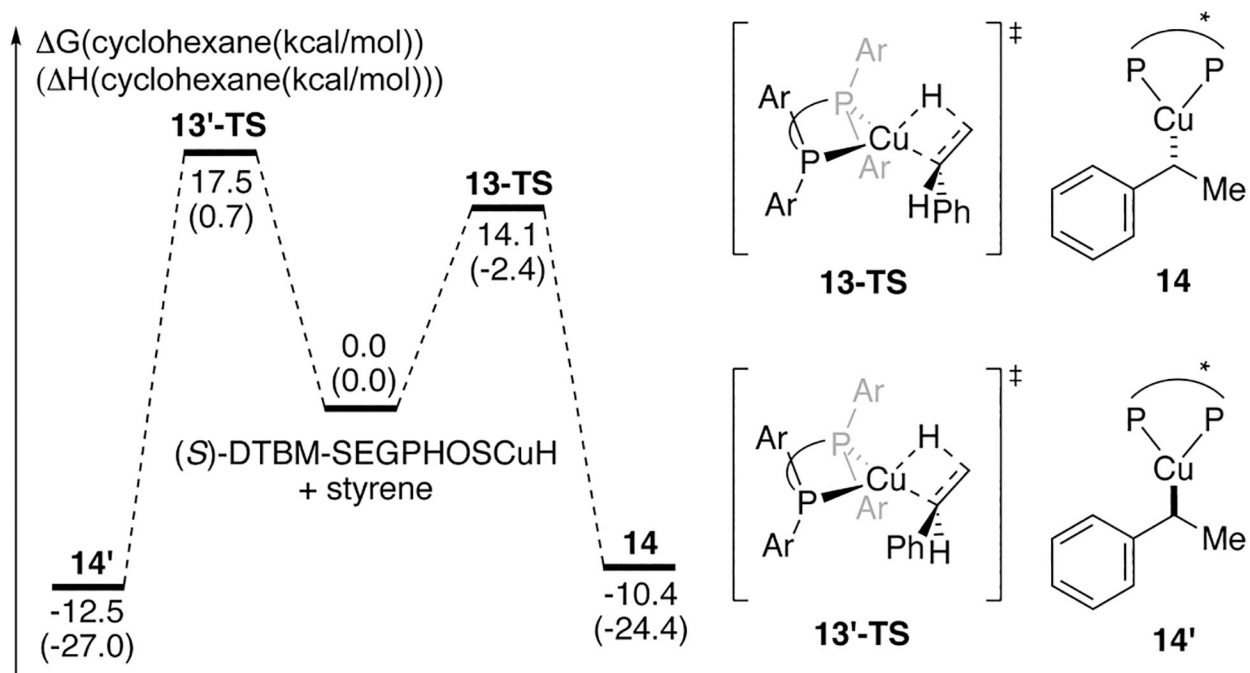
<sup>a</sup>Conditions: (A) 5 mol % CuCl, 10 mol % KO*t*Bu, 5.5 mol % (*S*)-SEGPHOS, toluene, rt, 54 h; (B) 2 mol % CuCl, 4 mol % KO*t*Bu, 2.2 mol % (*S*)-DTBM-SEGPHOS, cyclohexane, rt, 1 h; (C) 5 mol % CuCl, 10 mol % KO*t*Bu, 5.5 mol % (*S*)-SEGPHOS, cyclohexane, rt, 48 h; (D) 2.5 mol % CuCl, 5 mol % KO*t*Bu, 3 mol % (*S*)-DTBM-SEGPHOS, cyclohexane, rt, 36 h. GC yields. See Supporting Information for details.

**Scheme 3.**Proposed Synthesis of 5<sup>a</sup><sup>a</sup>The ancillary ligand on **5–8** is (*S*)-DTBM-SEGPHOS.

**Scheme 4.**

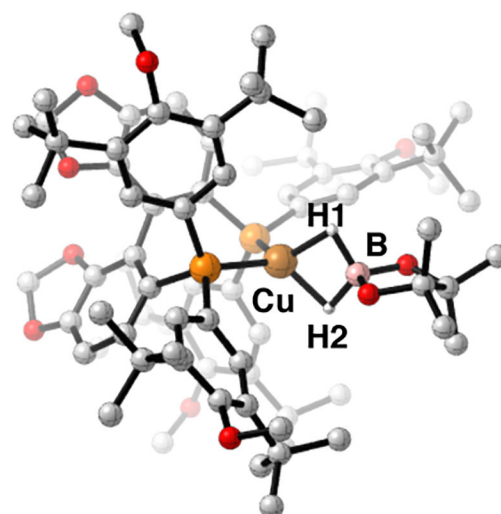
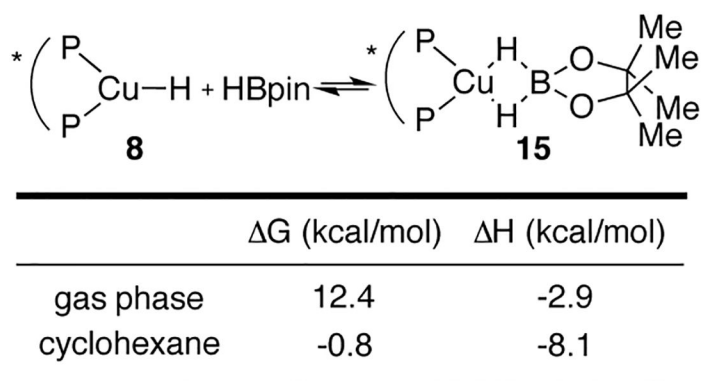
Synthesis of Phenethylcopper Complexes and Their Diastereomers<sup>a</sup>

<sup>a</sup>The ancillary ligand on **5** and **9–12** is (*S*)-DTBM-SEGPHOS. Yields were determined by NMR spectroscopy using an internal standard. The ratio in parentheses refers to the ratio of the two diastereomers.

**Scheme 5.**

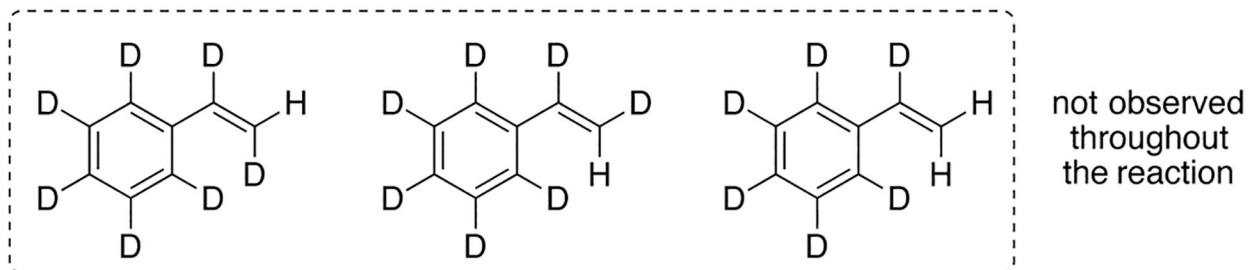
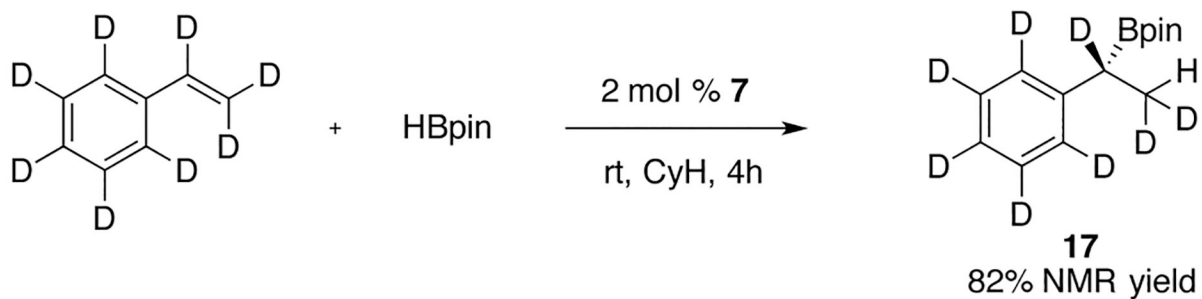
Pathways for Insertion of Styrene into LCu-H Bond Calculated by DFT Computations<sup>a</sup>

<sup>a</sup> Calculations were carried out at the M06/6-311+g-(d,p)/SDD//B3LYP/6-31g(d)/SDD level of theory.

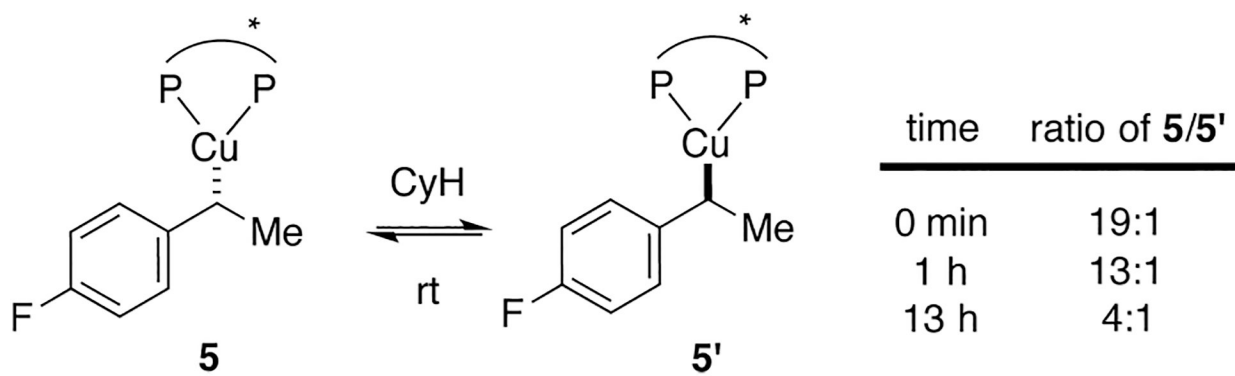
**Scheme 6.**

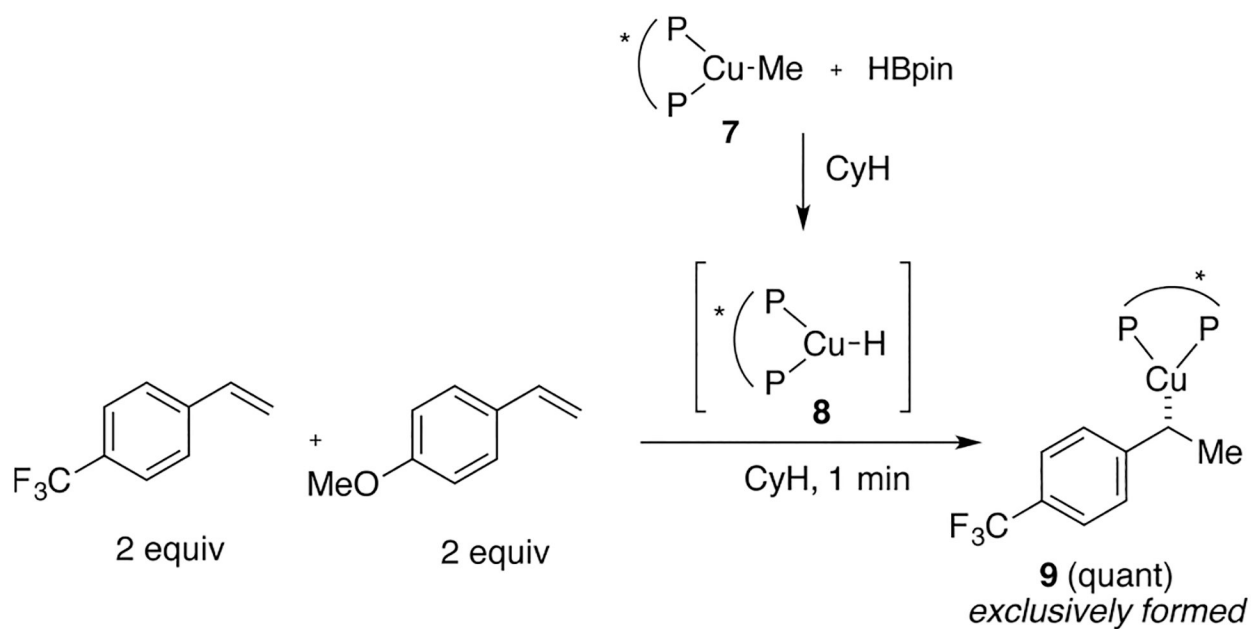
DFT Calculation of the Structure of Dihydridoborate Complex 15 and the Equilibrium for Dissociation of 15 to Copper Hydride 8 and HBpin<sup>a</sup>

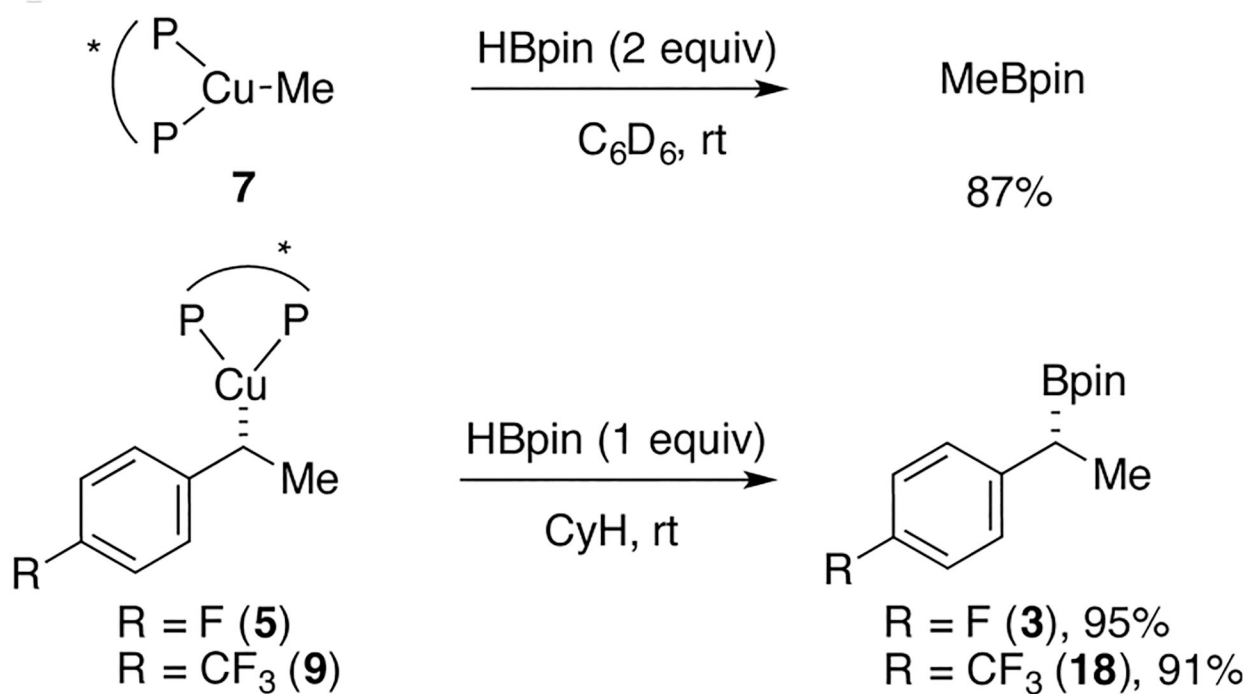
<sup>a</sup>Calculations were carried out at the M06/6-311+g-(d,p)/SDD//B3LYP/6-31g(d)/SDD level of theory. All hydrogen atoms that are bound to carbon atoms were omitted for clarity.



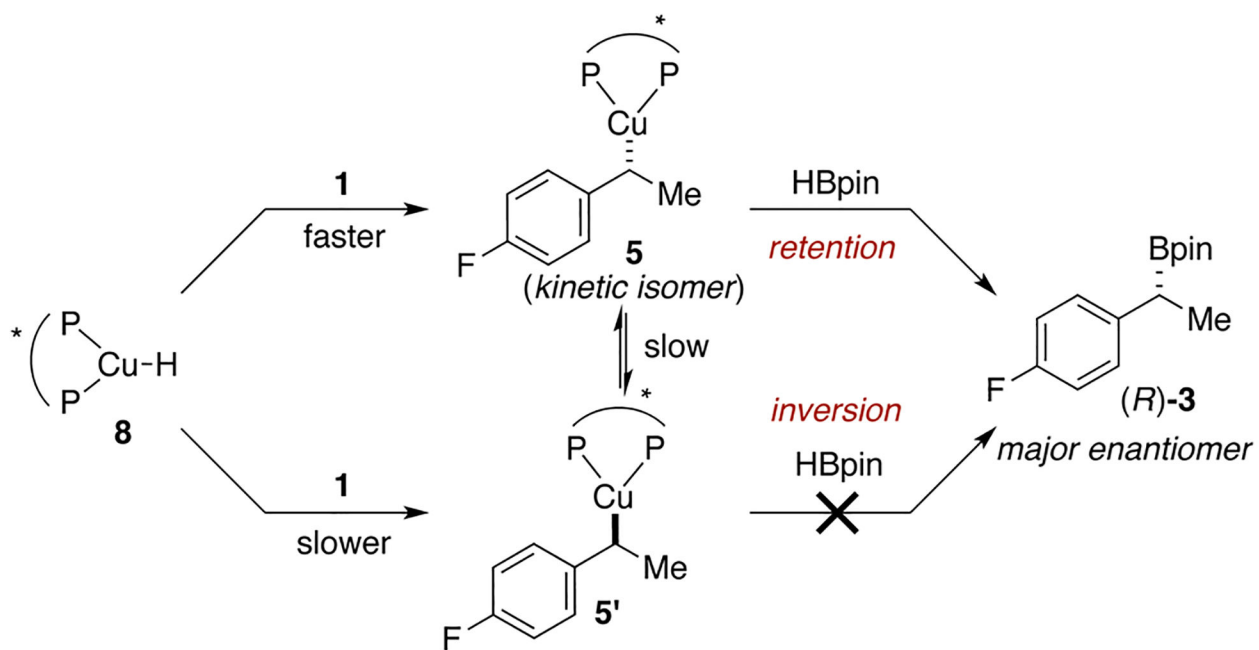
**Scheme 7.**  
Hydroboration of Styrene- $d_8$  with HBpin

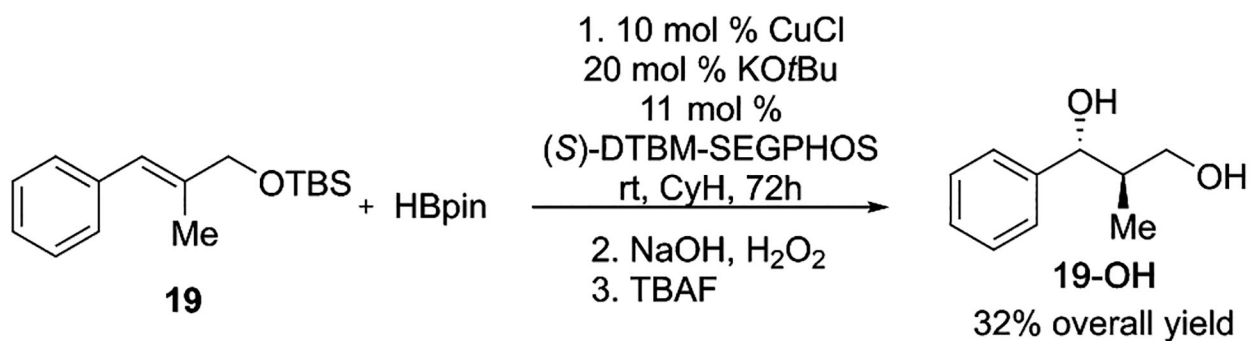
**Scheme 8.**Epimerization of Phenethylcopper **5** to **5'** in Solution<sup>a</sup><sup>a</sup>The ancillary ligand on **5** and **5'** is (*S*)-DTBM-SEGPHOS. The ratio was determined by <sup>19</sup>F NMR spectroscopy.

**Scheme 9.**Competition Experiments for Alkene Insertion into Copper Hydride **8**<sup>a</sup><sup>a</sup>The ancillary ligand on **7–9** is (*S*)-DTBM-SEGPHOS.

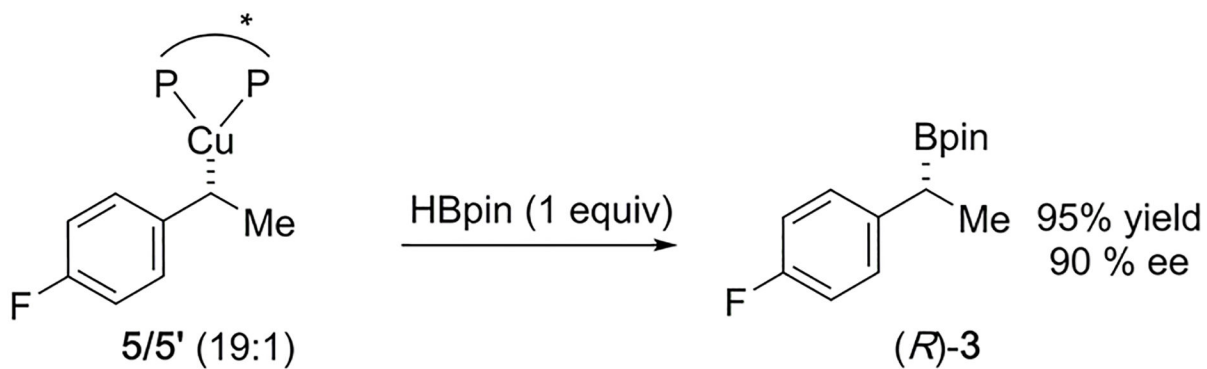


**Scheme 10.**  
Stoichiometric Reaction of Alkylcopper Complexes and HBpin<sup>a</sup>  
<sup>a</sup>The ancillary ligand on **5**, **7**, and **9** is (*S*)-DTBM-SEGPHOS.

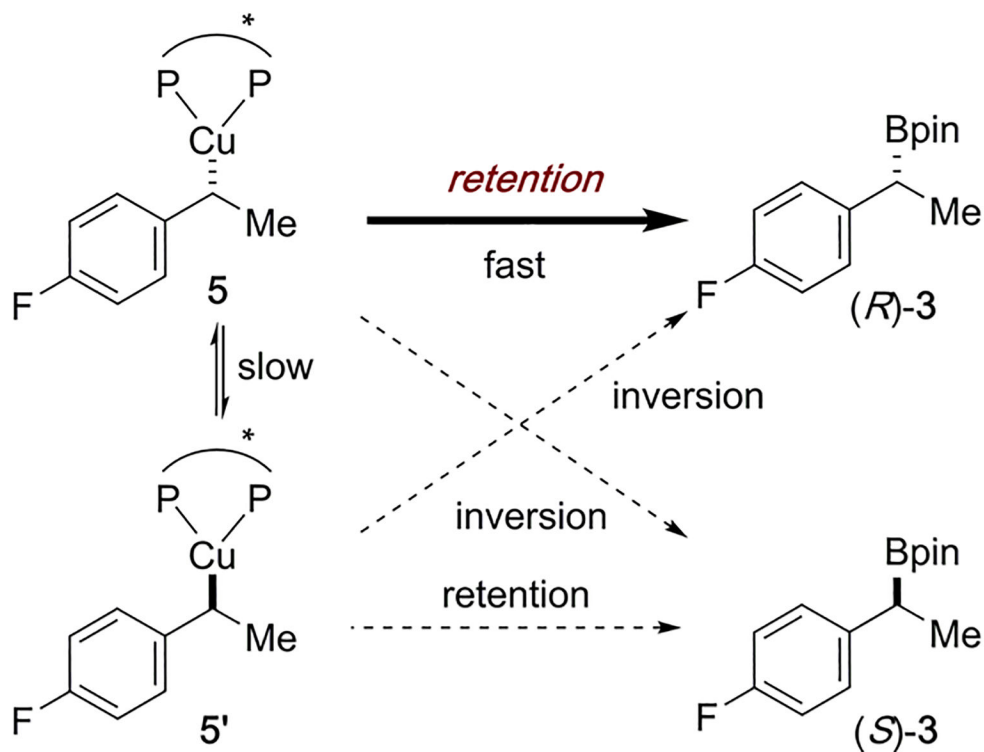
**Scheme 11.**Origin of the Major Enantiomer of the Hydroboration of Vinylarene 1<sup>a</sup><sup>a</sup>The ancillary ligand on **5**, **5'**, and **8** is (*S*)-DTBM-SEGPHOS.

**Scheme 12.**

Stereochemical Outcome of the Hydroboration of Trisubstituted Alkene 19



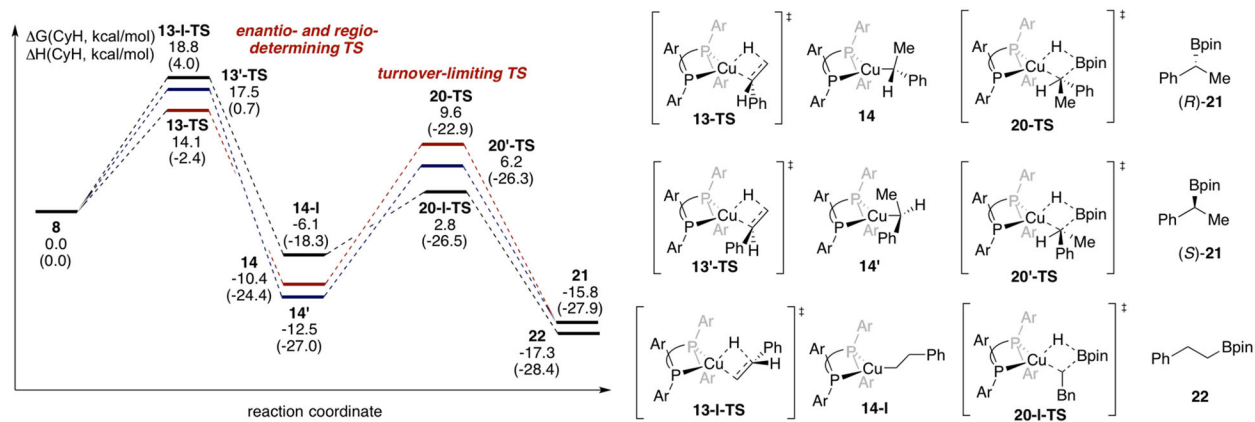
Possible mechanisms:



**Scheme 13.**

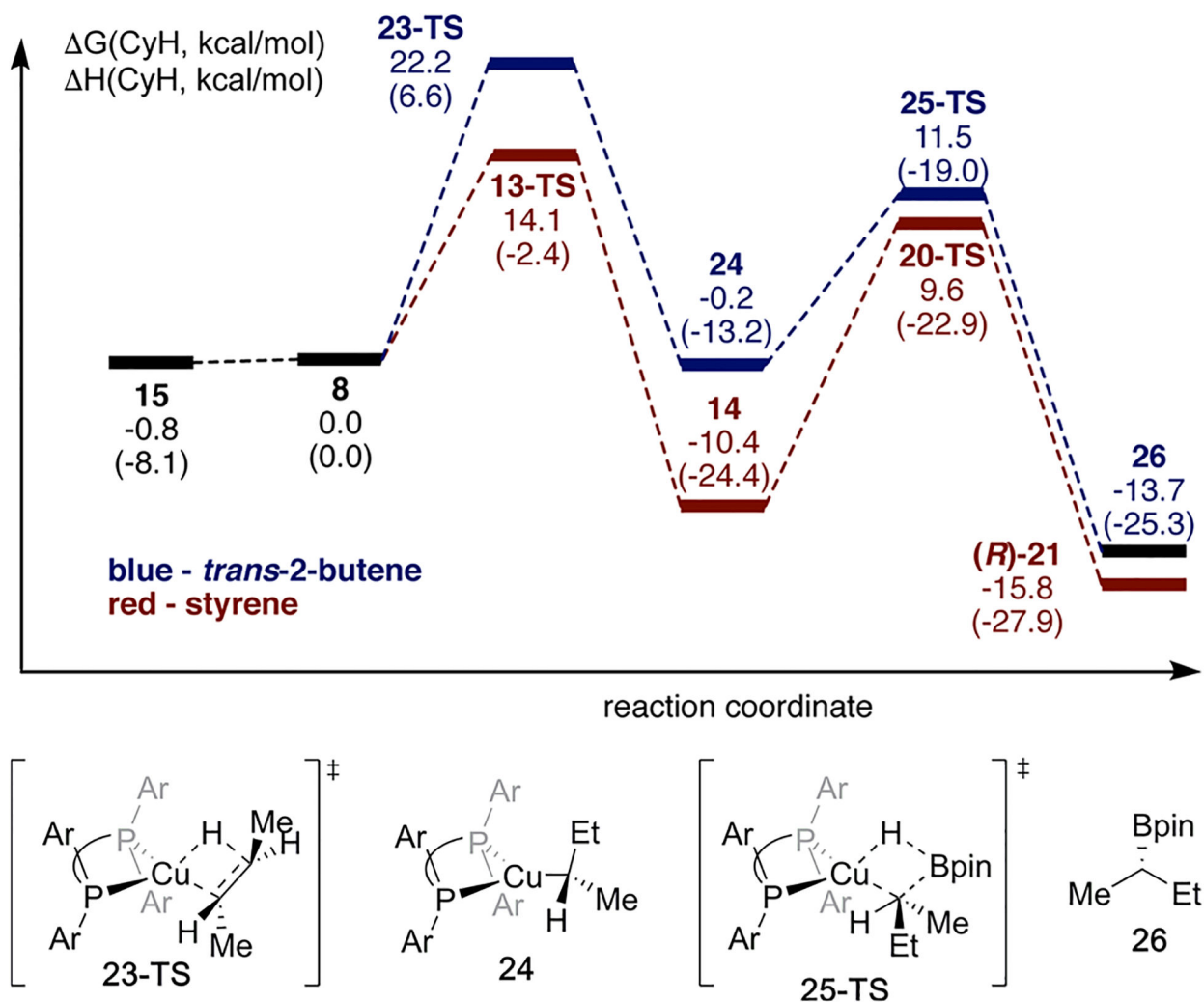
Stereochemical Outcome of the Borylation of Phenethylcopper 5<sup>a</sup>

<sup>a</sup>The ancillary ligand on **5** and **5'** is (*S*)-DTBM-SEGPHOS.

**Scheme 14.**

Computed Energy Surface for the Hydroboration of Styrene Catalyzed by a DTBM-SEGPHOS-Ligated Copper Complex Leading to All Possible Isomeric Products<sup>a</sup>

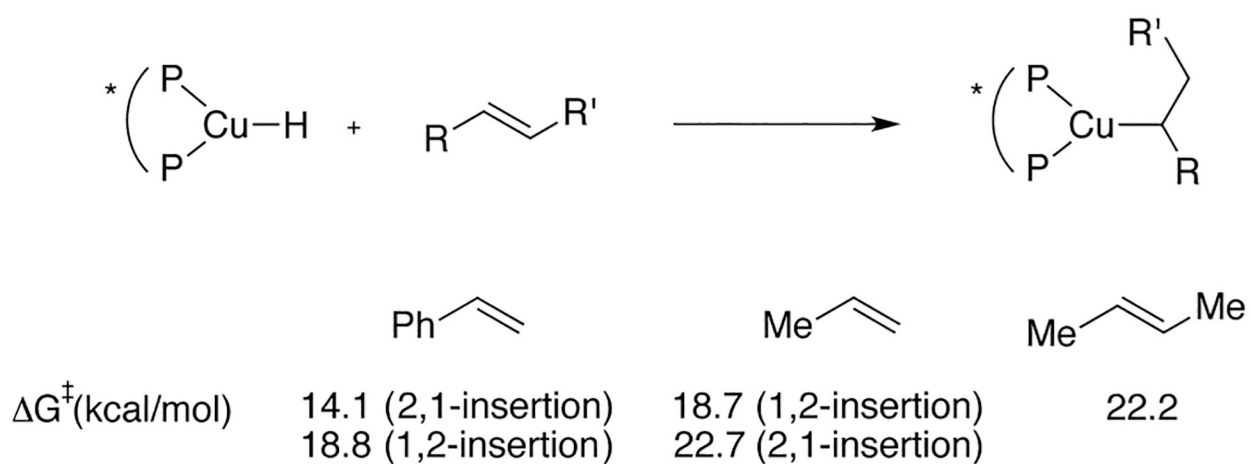
<sup>a</sup>The ancillary ligand is (*S*)-DTBM-SEGPHOS. See Supporting Information for computational details.



Scheme 15.

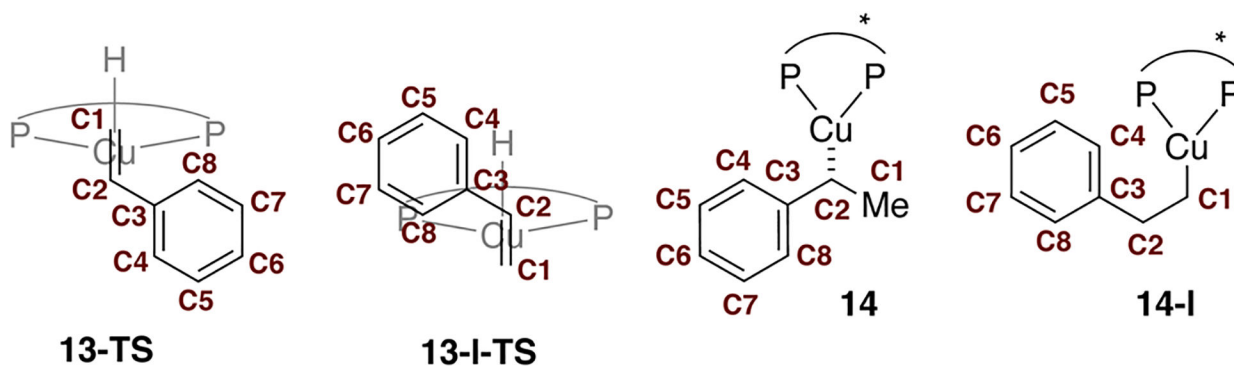
Computed Energy Surface for the Hydroboration of Styrene and *trans*-2-Butene<sup>a</sup>

<sup>a</sup>The ancillary ligand is (*S*)-DTBM-SEGPHOS. See Supporting Information for computational details.

**Scheme 16.**

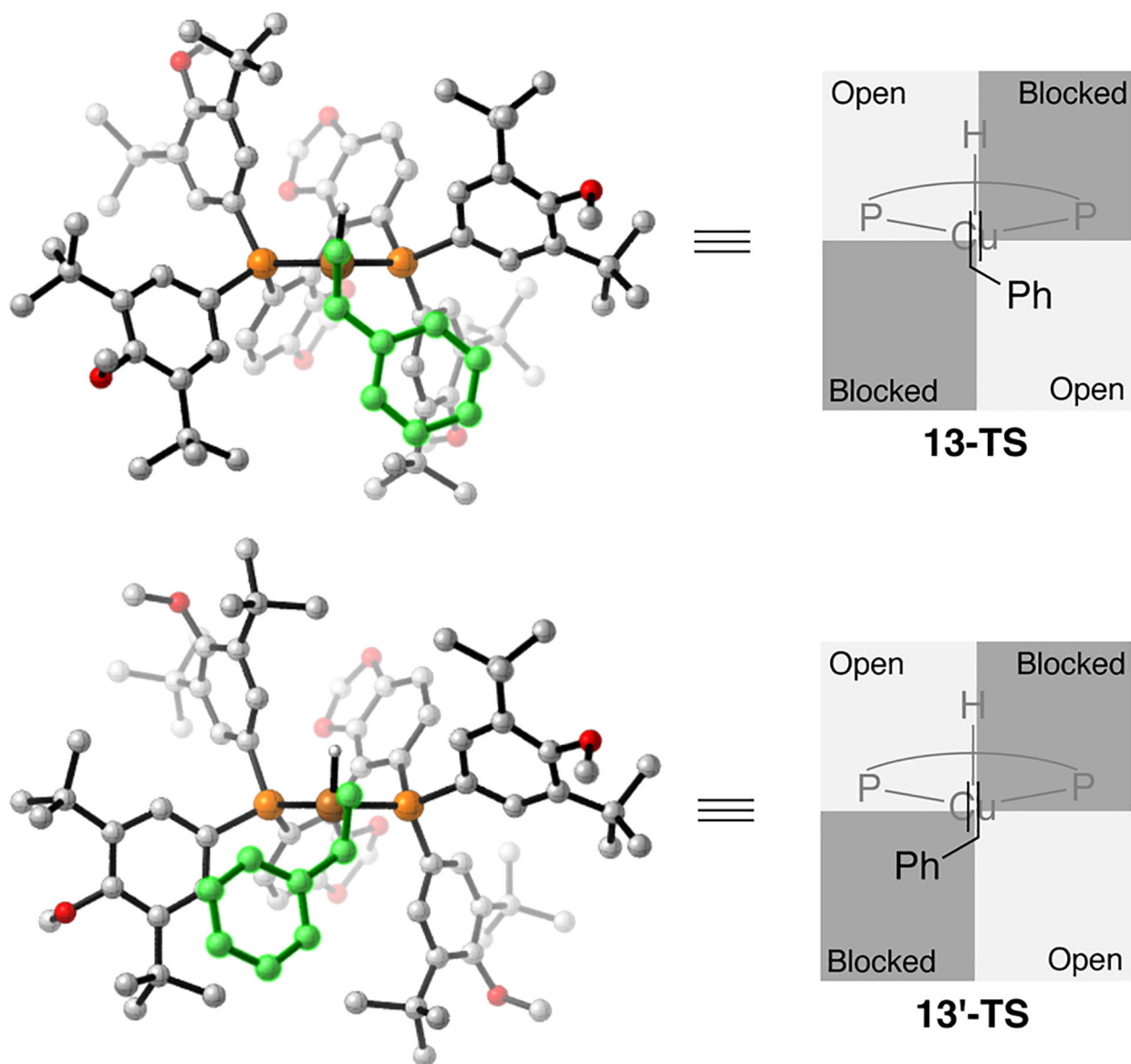
Activation Energies of Insertion of Various Alkenes Computed by DFT Calculations<sup>a</sup>

<sup>a</sup>The ancillary ligand is (*S*)-DTBM-SEGPHOS.



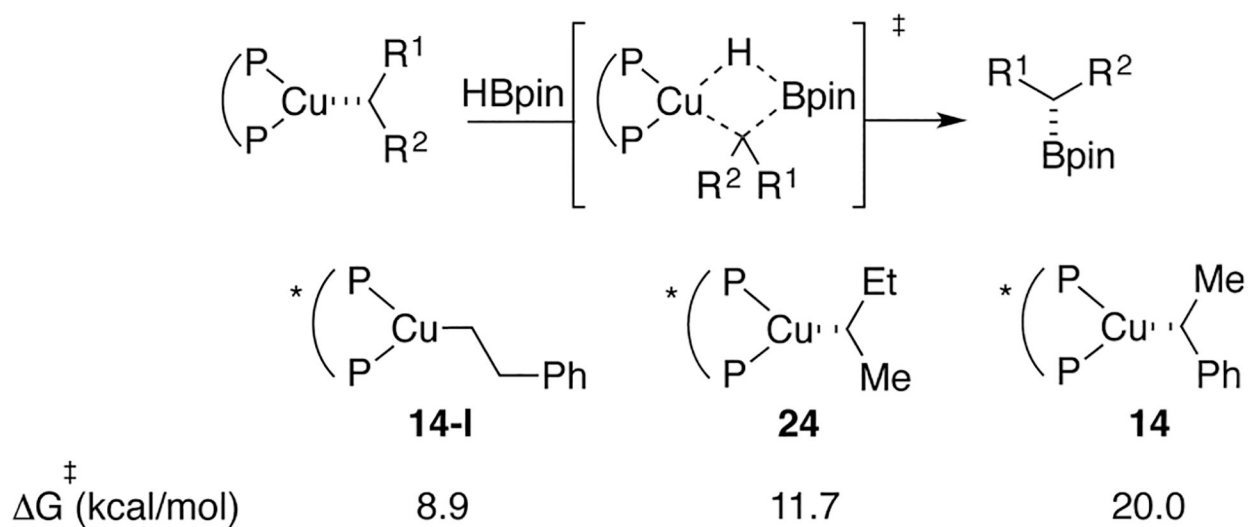
	C1	C2	C3	C4	C5	C6	C7	C8
<b>13-TS</b>	-0.067	-0.236	-0.019	-0.039	0.005	-0.055	0.002	-0.039
<b>13-I-TS</b>	-0.269	-0.085	-0.035	-0.005	0.005	-0.018	0.007	-0.003
styrene	0.022	0.002	-0.077	0.018	0.008	0.003	0.006	0.018
<b>14</b>	-0.015	-0.471	-0.002	-0.043	-0.003	-0.060	-0.001	-0.044
<b>14-I</b>	-0.550	-0.022	-0.007	-0.005	0.000	-0.024	-0.007	-0.019

**Scheme 17.**NBO Analysis of 13-TS, 13-I-TS, 14, and 14-I<sup>a</sup><sup>a</sup>The ancillary ligand is (*S*)-DTBM-SEGPHOS. NBO charges of hydrogen atoms were summed to those of the carbon atoms they are bound to.

**Scheme 18.**

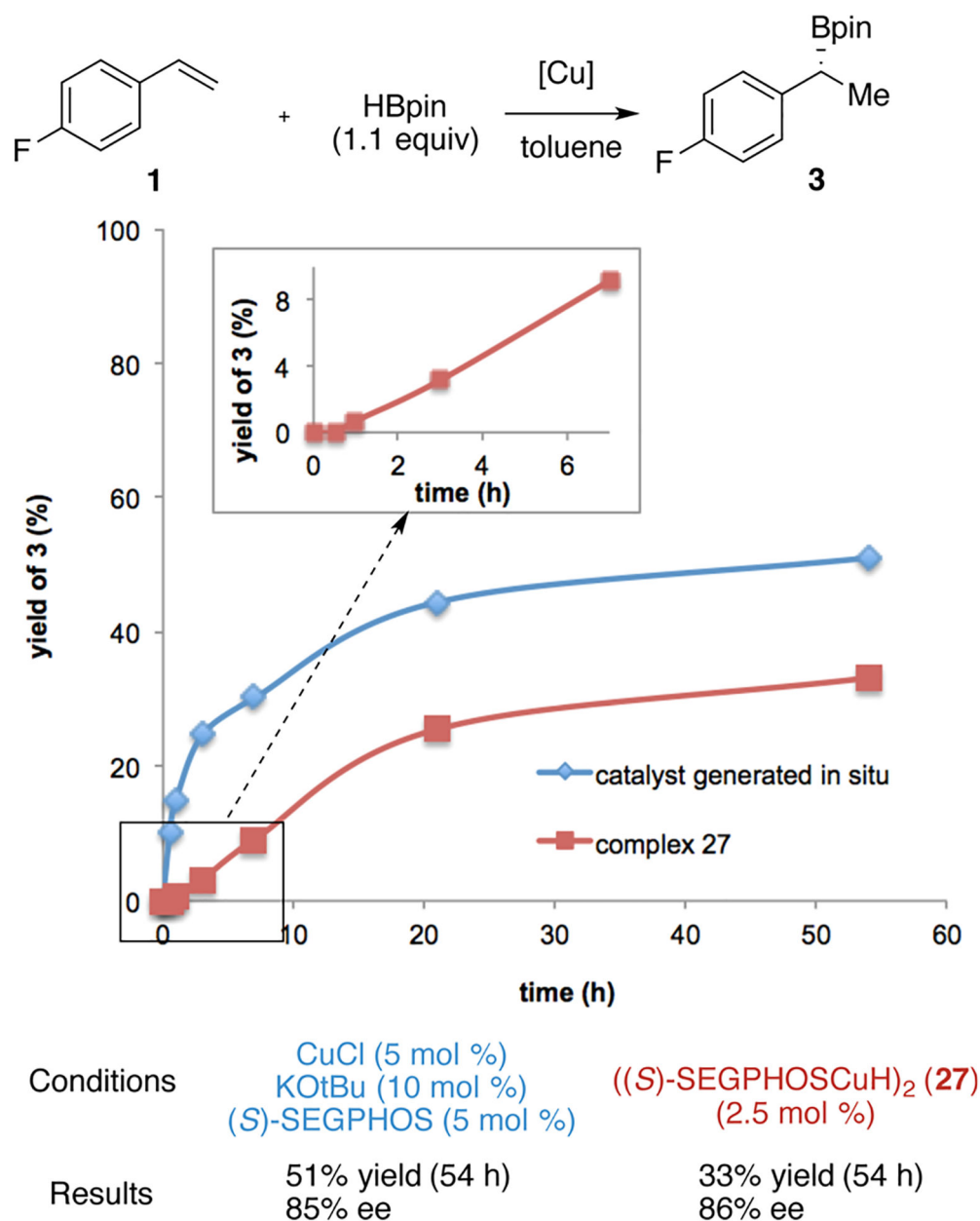
DFT Computed Structures and Quadrant Diagrams of Transition States 13-TS and 13'-TS<sup>a</sup>

<sup>a</sup>All hydrogen atoms that are bound to carbon atoms were omitted for clarity. The styrene moiety in the computed structures is highlighted in green.

**Scheme 19.**

Activation Energies of Borylation of Various Alkylcopper Intermediates Computed by DFT Calculations<sup>a</sup>

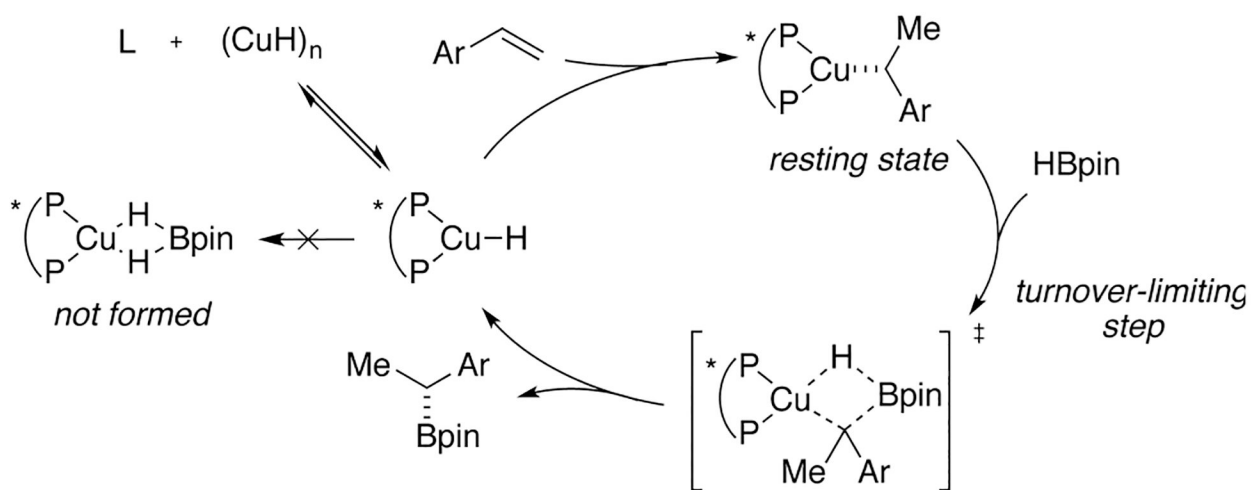
<sup>a</sup>The ancillary ligand is (*S*)-DTBM-SEGPHOS.



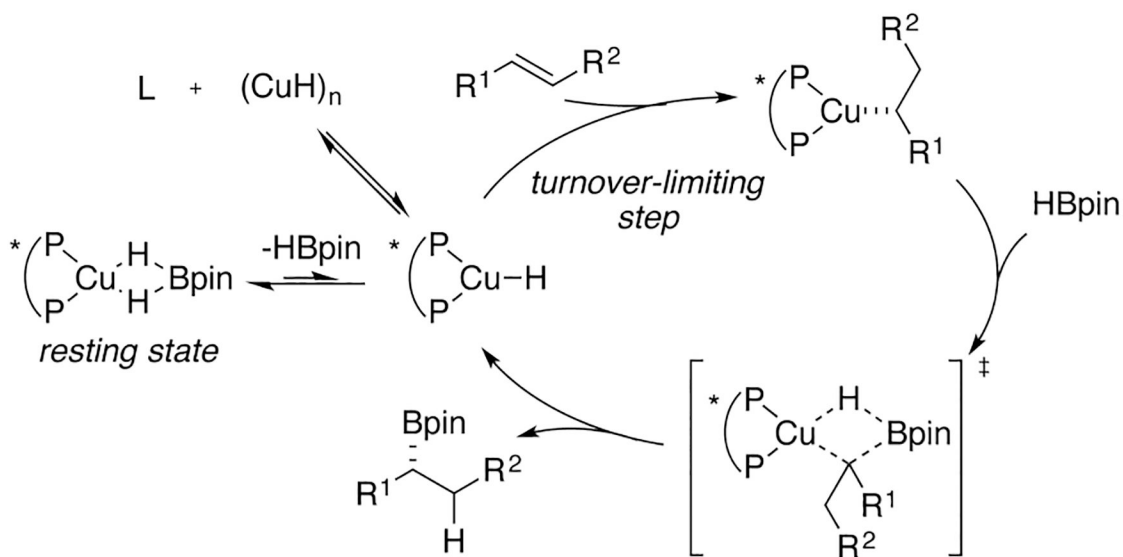
Scheme 20.

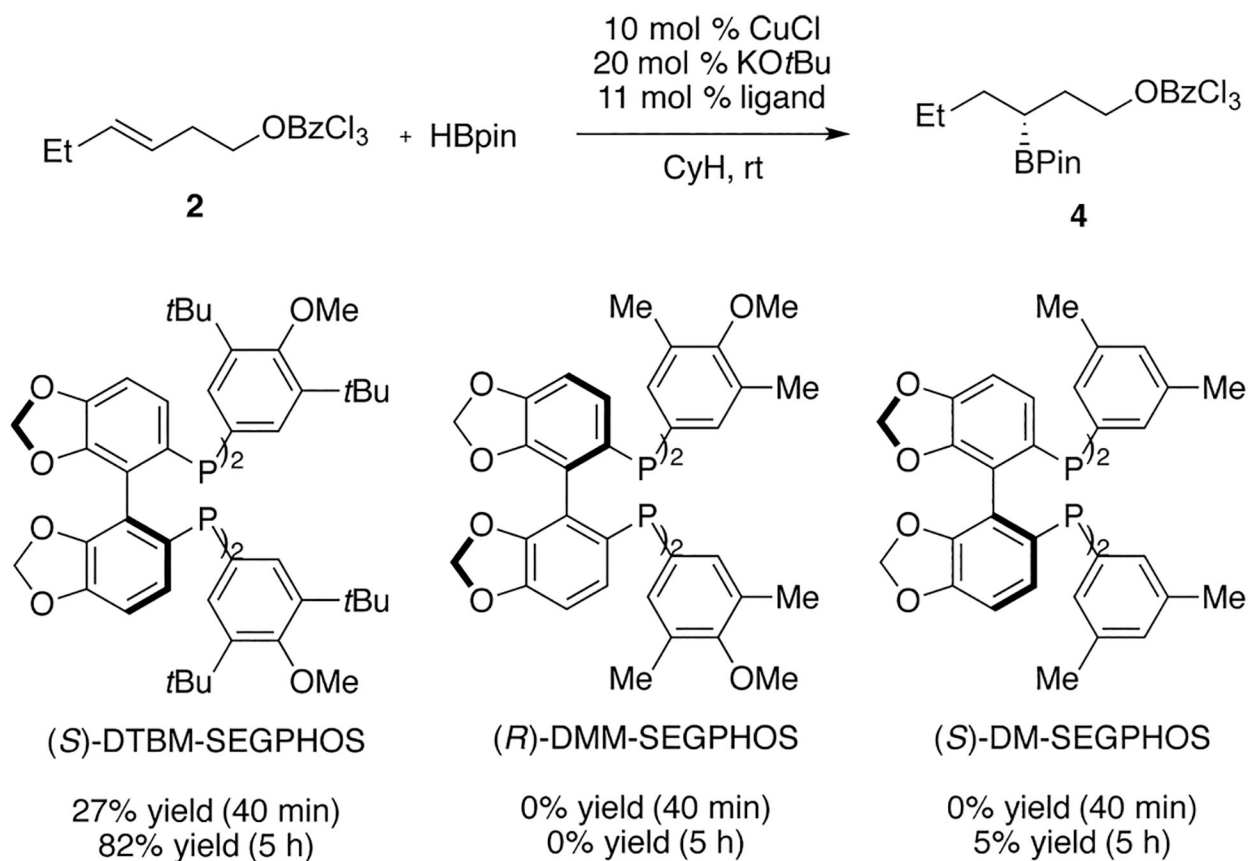
Assessment of the Catalytic Competency of Dimeric Hydride Complex 27

## A) Proposed mechanism for hydroboration of styrenes



## B) Proposed mechanism for hydroboration of internal alkenes

**Scheme 21.**Proposed Mechanism of Copper-Catalyzed Hydroboration<sup>a</sup><sup>a</sup>The ancillary ligand is (*S*)-DTBM-SEGPHOS.



**Scheme 22.**  
Evaluation of Ligands for the Hydroboration of 2